THE PERFORMANCE OF FRACTURED HORIZONTAL WELL IN TIGHT GAS RESERVOIR

A Dissertation

by

JIAJING LIN

Submitted to the Office of Graduate Studies of
Texas A&M University
in partial fulfillment of the requirements for the degree of

DOCTOR OF PHILOSOPHY

December 2011

Major Subject: Petroleum Engineering

The Performance of Fractured Horizontal Well in Tight Gas Reservoir

THE PERFORMANCE OF FRACTURED HORIZONTAL WELL

IN TIGHT GAS RESERVOIR

A Dissertation

by

JIAJING LIN

Submitted to the Office of Graduate Studies of
Texas A&M University
in partial fulfillment of the requirements for the degree of

DOCTOR OF PHILOSOPHY

Approved by:

Chair of Committee,	Ding Zhu
Committee Members,	A. Daniel Hill
	Ahmad Ghassemi
	Guy Battle
Head of Department,	Stephen A. Holditch

December 2011

Major Subject: Petroleum Engineering

ABSTRACT

The Performance of Fractured Horizontal Well in Tight Gas Reservoir.

(December 2011)

Jiajing Lin, B.S., Beijing Institute of Technology;

M.S., University of Louisiana at Lafayette

Chair of Advisory Committee: Dr. Ding Zhu

Horizontal wells have been used to increase reservoir recovery, especially in unconventional reservoirs, and hydraulic fracturing has been applied to further extend the contact with the reservoir to increase the efficiency of development. In the past, many models, analytical or numerical, were developed to describe the flow behavior in horizontal wells with fractures. Source solution is one of the analytical/semi-analytical approaches. To solve fractured well problems, source methods were advanced from point sources to volumetric source, and pressure change inside fractures was considered in the volumetric source method. This study aims at developing a method that can predict horizontal well performance and the model can also be applied to horizontal wells with multiple fractures in complex natural fracture networks. The method solves the problem by superposing a series of slab sources under transient or pseudosteady-state flow conditions. The principle of the method comprises the calculation of semi-analytical response of a rectilinear reservoir with closed outer boundaries.

A statistically assigned fracture network is used in the study to represent natural fractures based on the spacing between fractures and fracture geometry. The multiple dominating hydraulic fractures are then added to the natural fracture system to build the physical model of the problem. Each of the hydraulic fractures is connected to the horizontal wellbore, and the natural fractures are connected to the hydraulic fractures through the network description. Each fracture, natural or hydraulically induced, is treated as a series of slab sources. The analytical solution of superposed slab sources provides the base of the approach, and the overall flow from each fracture and the effect between the fractures are modeled by applying superposition principle to all of the fractures. It is assumed that hydraulic fractures are the main fractures that connect with the wellbore and the natural fractures are branching fractures which only connect with the main fractures. The fluid inside of the branch fractures flows into the main fractures, and the fluid of the main fracture from both the reservoir and the branch fractures flows to the wellbore.

Predicting well performance in a complex fracture network system is extremely challenged. The statistical nature of natural fracture networks changes the flow characteristic from that of a single linear fracture. Simply using the single fracture model for individual fracture, and then adding the flow from each fracture for the network could introduce significant error. This study provides a semi-analytical approach to estimate well performance in a complex fracture network system.

DEDICATION

To my parents,

Gang Lin and Yingcai Wu,

my husband, Xuehao Tan

for their love and support

ACKNOWLEDGEMENTS

Although this dissertation would not have been possible without the help of many people, my first gratitude would go to my adviser, Dr. Ding Zhu. I would like to express my sincere appreciation to Dr. Zhu for giving me the opportunity to pursue my Ph.D. at Texas A&M University. I am grateful to her commitment and encouragement throughout my study. Her guidance, patience, and generosity made me where I am today.

My truthful gratitude is extended to my committee members, Dr. Hill, Dr. Ghassemi and Dr. Battle for their suggestions and comments on my dissertation. I would like to especially thank Dr. Hill for his valuable advice and his generosity.

The degree and dissertation could not be completed without my husband, Xuehao Tan, who always loved and supported me. I deeply appreciate his dedication and time during my graduate study. I cannot imagine how I could have graduated without him, and he definitely deserves this honor as much as I do.

Thanks also go to my friends and colleagues and the department faculty and staff for making my time at Texas A&M University a great experience. I would like to thank the Crisman Research for providing the financial support for the project.

Finally, thanks to my mother and father for their love.

TABLE OF CONTENTS

Page

LIST OF TABLES

Page

LIST OF FIGURES

Page

Page

Page

CHAPTER I

INTRODUCTION

1.1 Statement of the Problem

In recent years, hydrocarbon resources recoverable from reservoirs of different natures have become important play. These resources are referred as "unconventional resources", including tight gas, gas/oil shale, oil sands, and coal-bed methane. North America has a substantial growth in its unconventional oil and gas market over the last two decades. The primary reason for that growth is because North America, being a mature market, is beyond the peak production from its convention hydrocarbon resources.

The defining characteristics of an unconventional resource are at best nebulous. Etherington (2005) states "An unconventional reservoir is one that cannot be produced at economic flow rates without assistance from massive stimulation treatments or special recovery processes." Others use a definition based upon two common aspects, they are comprised of large volumes of rock pervasively charged with hydrocarbon, and that the accumulation types are not dependent on buoyancy.

This dissertation follows the style of *SPE Production & Operations.*

New technology applications of multi-fractured horizontal wells allow us to produce at economical rates from these low permeable oil and gas resources. Since commercial exploration and production of oil and gas reservoirs began there have been circumstances where the reservoir character or depositional model has caused difficulty in assessment. Production assessment of unconventional reservoirs using standard methodology has been notoriously problematic. The complexity of the fractured system posts the challenges to analytical models, and reservoir simulation of such a system is extremely time-consuming.

Although most of the solutions to the flow problem in porous media have been investigated in a similar case as in the heat transfer and the solution is originated from the heat transfer, Gringarten and Ramey's (1973) work is the first application of the Green's and Source function to the problem of unsteady-state fluid flow in the reservoirs. They introduced proper Green's functions for a series of source shapes and boundary conditions. They showed that the point source solution is actually a more general theory of Green's function, and used the integration of the response to an instantaneous source solution to get the response for a continuous source solution. The application of the Newman's principle in breaking a problem of 3D into the product of three 1 D solutions is also discussed in this work.

The application of source and Green's function later extended to the unsteady-state pressure distribution for more complex well completion schematics by others. The major disadvantage of this method is the inherent singularity of the solution wherever the source is placed. Since the source is assumed to have no volume (point, line source), the

source is considered to be at infinite pressure at the time zero and it is not possible to calculate the exact pressure as a function of time at the point where source is placed. To handle this problem, a source method with assigned volume needs to be developed.

Furthermore, as the petroleum industry goes toward producing lower quality reservoirs like low- and ultra-low permeability reservoirs, the period of transient flow covers larger part of the well lifetime and these pseudosteady-sate productivity calculations become less applicable in prediction of the reservoir's production behavior. A source method needed to be able to fill this gap.

1.2 Objectives

In this proposed research, we present a different approach to the problem of unsteady state flow of a compressible fluid in a rectilinear reservoir. The model is based on the solution of a series of slab sources. It can be used to calculate well performance for horizontal gas wells with or without fractures. Fractures can be longitudinal or transverse, single or multiple, and fractures can be infinite conductivity or uniform influx. Using the slab source approach, we assigned the sources (horizontal wells or fractures) a geometry dimension and the effect of pressure behavior inside sources are considered by superposition principles. This method is relatively easy to apply because flow rate could be calculated directly from pressure difference between initial reservoir

pressure and pressure in fracture, which is the same as wellbore flow pressure for an infinite conductivity fracture.

The research proposed in this project will develop a model to predict fractured horizontal well performance in tight/shale gas reservoirs. It will accomplish the flowing objectives.

1. To develop the slab source method as a solution to the problem of pressure and production distribution in a closed, rectangular reservoir for a uniform flux boundary condition.
2. To validate a series of solutions for pressure and flow rate behavior of simple and complex well/fracture configurations such as:
    - Vertical well
    - Horizontal well
    - Multiple fractures along a horizontal well
    - Hydraulic fractured well with natural fractures
3. To demonstrate the applicability of the new solution method in predicting pressure and production behavior for a complex well/fracture configuration.
4. To apply the new method as an optimization tool to obtain the best completion schematic for development of an example case.
5. To study the flow effect inside of fractures by dividing the fracture into several segments.

1.3 Literature Review

Over the past decades, point source integrated over a line and/or a surface has been mostly used in solving single-phase flow problems in porous media when fluid movement is from a complex fractured well system, Horizontal well models with point source solution have been presented in many literatures.

Gringarten and Ramey (1973) were the first to apply the Green's and source function to the reservoir flow problems. They introduced Green's function under different boundary conditions for plane, slab, line, and point source. The source function is combined with Newman's product to de-component a problem in 3D to the product of three 1D solutions.

Gringarten et al. (1974) applied the Green's function later to the unsteady state pressure distribution created by a vertical fractured well with infinite conductivity fracture. By dividing the fracture into N segments, a series of equations had been solve to calculate the pressure distribution and contribution of each segment to the total flow by assuming each segment as a uniform flux source.

Cinco-Ley and Samaniego (1981) used the Green's function under Laplace transform to develop the model of finite conductivity vertical fracture in an infinite reservoir. They presented a new technique for performing pressure transient analysis for vertical finite-conductivity fractures using a bilinear flow model.

Point source solution was introduced by Ozkan et al. (1995). He developed point source solution in Laplace domain in order to remove the limitations of the Gringarten and Ramey's model in considering the wellbore storage and skin effects.

By integrate the point source to line source, Babu and Odeh (1988) developed a line source solution to predict horizontal well performance in a closed reservoir. The model is under pseudosteady-state condition. One of the limitations of this method is the well must be parallel to the reservoir boundary.

Goode and Kuchuk (1991) introduced solution for productivity of a horizontal well in a reservoir with no-flow boundary and constant pressure boundary. Their solution is expressed in the form of an infinite condition. A simplified solution for a short well was developed in their study.

Ouyang et al. (1997) presented a 3D horizontal well model to describe wellbore pressure and reservoir pressure change with time and location. The formula is in the Laplace space. The transient pressure behaviors in physical space can be easily obtained by means of the Stehfest algorithm.

Valko and Amini (2007) developed a method with distributed volume sources to simulate fractured horizontal wells in a box-shaped reservoir. A source term was added to the diffusivity equation to calculate the pressure distribution. Then the production rate from a fracture is computed. Different from the other point source methods, the volume source approach is able to describe the pressure behavior inside sources and its influence to the flow field.

Zhu et al. (2007) showed applications of the volumetric source model and field cases are presented in their work.

Meyer et al. (2010) presented a comprehensive methodology using the trilinear solution to predicting the behavior of multiple transverse finite conductivity vertical fractures in horizontal wellbores.

Miskimins et al. (2005) demonstrated that non-Darcy flow effects can influence well productivity across the entire spectrum of flow rates, including low rates. They showed that even in low velocity situations, non-Darcy effects can influence the productivity. Non-Darcy flow can have a major impact on reduction of a propped half-length to a considerably shorter effective half length, thus lowering the well's productive capability and overall reserve recovery.

CHAPTER II

METHODOLOGY

Point source and line source solutions have been used to solve petroleum engineering problems in past years. The model is adapted from point source solutions of heat conduction problem. The slab source solution of 3D problems is obtained by multiplying three 1D slab sources together and integrating in time and along the source. This chapter presents a semi-analytical slab source solution for 3D wellbore and fracture system in this chapter. The model developed here can be applied to a variety of systems including horizontal wells, slanted wells, single fracture, and multiply fractures along a horizontal well. Firstly, the semi-analytical slab source solution is derived, and then the slab source solution is applied to predict well performance for different well systems. It also discusses the inner boundary conditions on the flow rate and wellbore pressure distribution along the wellbore and fractures. Finally, the non-Darcy effect inside of the fractures is studied.

2.1 Source Technique

The diffusivity equation of a single-phase incompressible fluid is written as Eq.(2.1)

$$\frac{\partial^2 p}{\partial x^2} = \frac{\phi \mu c_t}{k} \frac{\partial p}{\partial t} \tag{2.1}$$

For an anisotropic medium, the diffusivity in three directional domains becomes

$$k_x \frac{\partial^2 p}{\partial x^2} + k_y \frac{\partial^2 p}{\partial y^2} + k_z \frac{\partial^2 p}{\partial z^2} = \phi \mu c_t \frac{\partial p}{\partial t} \tag{2.2}$$

Because the diffusivity equation is in the same format as the heat conduction problems, we can directly apply the sink/source technique to solve the flow in porous media.

2.1.1 Instantaneous Point Source

Gringarten and Ramey (1973) presented the instantaneous Green's function in infinite plane reservoir. The geometries of the source function are shown in **Fig. 1** and Green's functions for different boundary conditions in infinite plane reservoirs are shown in **Table 1**.

Table 1—Instantaneous Green's function in 1D infinite reservoir.

Boundary Conditions	Instantaneous Green's functions for point source
Constant pressure at x=0 and x=a	$\frac{2}{a}\sum_{n=1}^{\infty}\sin\frac{n\pi x}{a}\sin\frac{n\pi x_0}{a}\exp\left[-\frac{n^2\pi^2 k_x \tau}{\alpha a^2}\right]$
No-Flow at x=0 and x=a	$\frac{1}{a}\left(1+2\sum_{n=1}^{\infty}\cos\frac{n\pi x}{a}\cos\frac{n\pi x_0}{a}\exp\left[-\frac{n^2\pi^2 k_x \tau}{\alpha a^2}\right]\right)$
No-Flow at x=0 Constant pressure at x=0	$\frac{2}{a}\left(\sum_{n=1}^{\infty}\cos\frac{(2n+1)\pi x}{a}\cos\frac{(2n+1)\pi x_0}{a}\exp\left[-\frac{(2n+1)^2\pi^2 k_x \tau}{4\alpha a^2}\right]\right)$

where, $\alpha = \phi \mu c_t$.

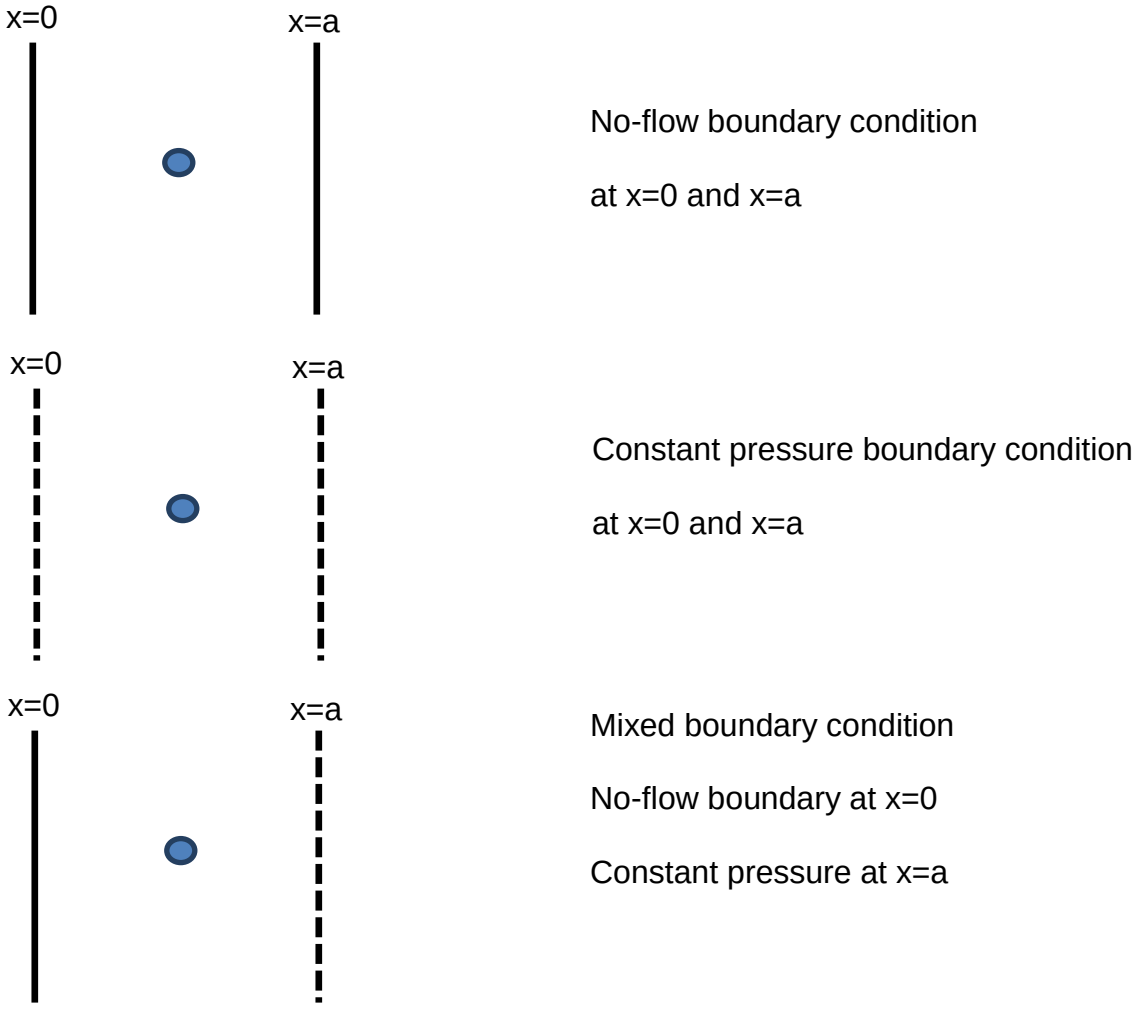

Fig. 1—Instantaneous Green's function for point source.

For a 3D problem Newman's product can be applied to instantaneous Green's and source functions which solves a 3D problem by multiplication of three 1D problem solution. The instantaneous Green's function for a 3D reservoir that can be visualized as the intersection of three one-dimensional reservoirs is equal to the product of the instantaneous Green's function for each one-dimensional reservoir. For example, the

dimensional pressure drop as a results of a constant production, q, at a position (x_0, y_0, z_0) in a homogenous box-shaped reservoir measured at a position (x,y,z) is readily calculated by

$$p_{\text{int}} - p(x,y,z,t) = \left[\frac{B\mu q}{L\alpha}\right](s_x s_y s_z) \tag{2.3}$$

In the above equation, pint is initial pressure, B is formation volume factor, L is the distance between point (x,y,z) and (x0,y0,z0), and sx, sy, and sz are the solution of 1D source problem depending on the instantaneous Green's functions which shown in **Table 1**. **Fig. 2** shows the geometry of the source and the reservoir.

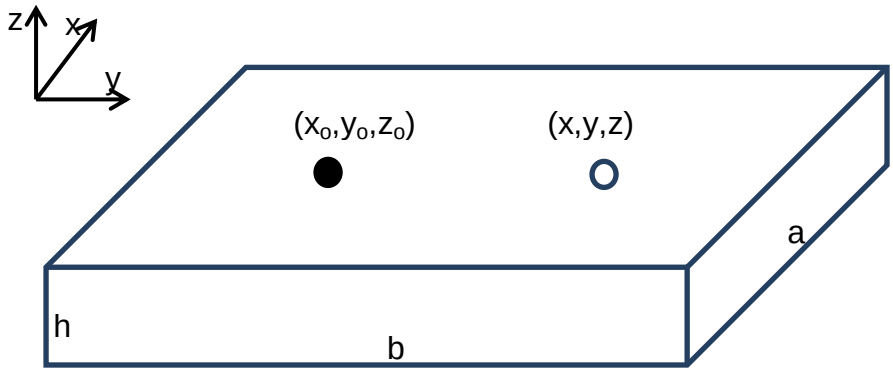

Fig. 2—Instantaneous point source in a box-shaped reservoir.

For example, if the reservoir is completely bounded or no-flow across the reservoir boundary, and s_x, s_y, and s_z in this case are

$$s_x = \frac{1}{a}\left(1 + 2\sum_{n=1}^{\infty} \cos\frac{n\pi x}{a}\cos\frac{n\pi x_0}{a}\exp\left[-\frac{n^2\pi^2 k_x \tau}{\alpha a^2}\right]\right) \tag{2.4}$$

$$s_y = \frac{1}{b}\left(1 + 2\sum_{m=1}^{\infty} \cos\frac{n\pi y}{b}\cos\frac{n\pi y_0}{b}\exp\left[-\frac{m^2\pi^2 k_y \tau}{\alpha b^2}\right]\right) \tag{2.5}$$

$$s_z = \frac{1}{h}\left(1 + 2\sum_{l=1}^{\infty} \cos\frac{n\pi z}{h}\cos\frac{n\pi z_0}{h}\exp\left[-\frac{l^2\pi^2 k_z \tau}{\alpha h^2}\right]\right) \tag{2.6}$$

2.1.2 Continuous Point Source Solution

By integrating the continuous point source solution along a line, the continuous line source solution could be developed. For a line source that have the initial position at (x_{01}, y_{01}, z_{01}) and the end point at (x_{02}, y_{02}, z_{02}) as shown in **Fig. 3**, the solution of the continuous line source in dimensional format can be written as,

$$p_{\text{int}} - p(x,y,z,t) = \int_{y_1}^{y_2}\int_{0}^{t}\left[\frac{B_0\mu_0 q_0}{L\alpha}\right](s_x s_y s_z)\,d\tau dy \tag{2.7}$$

The s_x, s_y, and s_z can be any combinations of the instantaneous Green's function depending on the boundary conditions in **Table 1**.

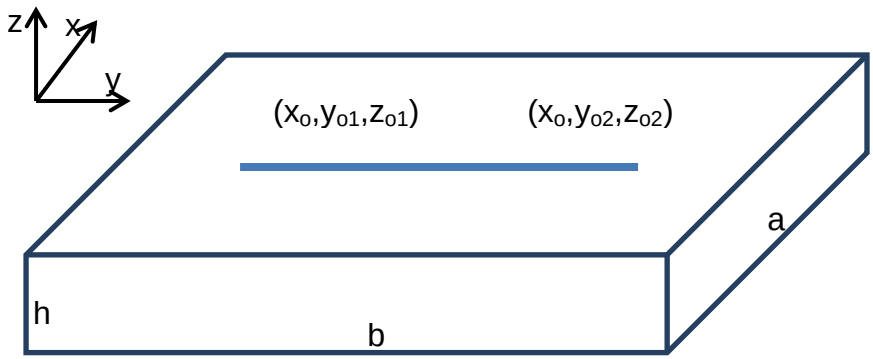

Fig. 3—Schematic of a horizontal well trajectory in line source.

2.1.3 Slab Source Solution

The slab source method solves the flow problem in a parallelepiped porous medium with a slab source, **s**, placed in the domain, as shown in **Fig. 4**. The reservoir is assumed to be an anisotropic porous medium. Following the same approach as the conventional point source solution to apply Newman's principle, the three-dimensional pressure response of the system to an instantaneous source can be obtained as the production of the solutions of three one-dimensional problems from each principal direction.

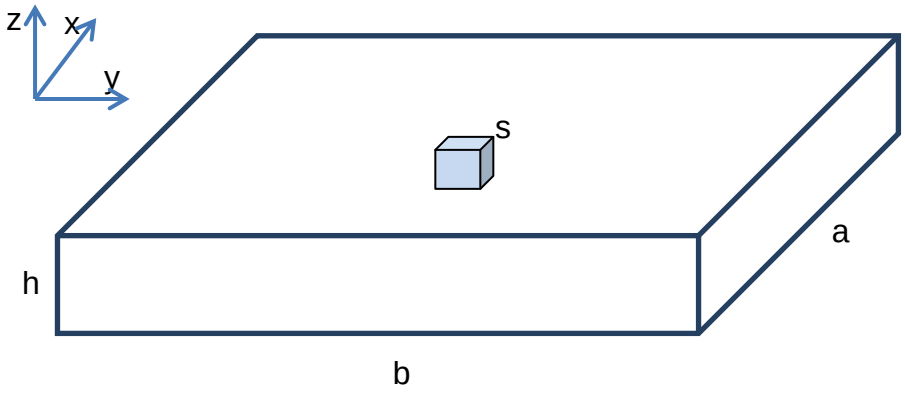

Fig. 4—Schematic of the slab source model.

The solution from this technique applies to different state in the flow period, both transient flow and stabilized flow. The boundary condition of the reservoir can be constant pressure boundary, no-flow boundary or mixed boundary, which makes the model practical to a wide range of flow problems in petroleum engineering.

The procedure of obtaining the solution is to obtain one-dimensional solution of the slab problem, applying Newman's product method based on instantaneous source function in an infinite reservoir to get three-dimensional solution, and then integrates the three-dimensional solution over time to get a continuous source function. Modifying the point source domain by placing a pair of parallel plates in the domain, as shown in **Fig. 5**, we began the model with one-dimensional instantaneous infinite slab source in an infinite slab reservoir. Green's functions (Carslaw and Jaeger, 1959) for different boundary conditions in infinite slab domain with a system schematic are shown in **Table 2**.

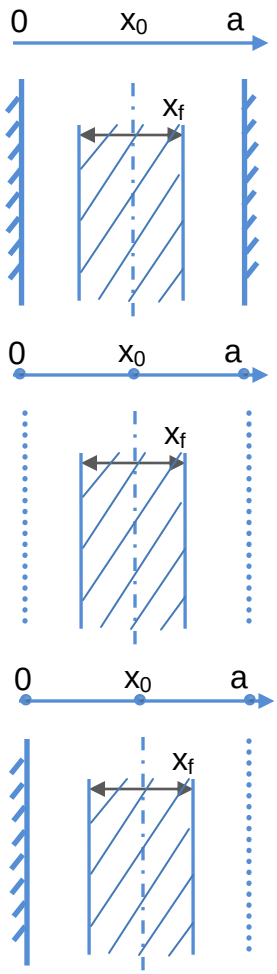

No-Flow boundary Condition

at x=0 and x=a

Constant pressure boundary Condition

at x=0 and x=a

Mixed boundary Condition

No-flow boundary at x=0

Constant pressure at x=a

Fig. 5—Instantaneous Green's function for slab source.

Table 2—Instantaneous Green's function in 1D infinite slab reservoir (Carslaw and Jaeger, 1959).

Boundary Conditions	Instantaneous Green's Functions
Constant pressure at x=0 and x=a	$\frac{4}{\pi}\sum_{n=1}^{\infty}\frac{1}{n}\sin\frac{n\pi x_f}{2a}\sin\frac{n\pi x_o}{a}\sin\frac{n\pi x}{a}\exp\left(-\frac{n^2\pi^2 k_x\tau}{a^2}\right)$
No-flow at x=0 and x=a	$\frac{x_f}{a}\left[1+\frac{4a}{\pi x_f}\sum_{n=1}^{\infty}\frac{1}{n}\sin\frac{n\pi x_f}{2a}\cos\frac{n\pi x_o}{a}\cos\frac{n\pi x}{a}exp\left(-\frac{n^2\pi^2 k_x\tau}{a^2}\right)\right]$
No-flow at x=0 Constant pressure at x=a	$\frac{8}{\pi}\sum_{n=1}^{\infty}\frac{1}{2n+1}\sin\frac{(2n+1)\pi x_f}{4a}\cos\frac{(2n+1)\pi x_o}{a}\cos\frac{(2n+1)\pi x}{a}$ $\exp\left(-\frac{(2n+1)^2\pi^2 k_x\tau}{4a^2}\right)$

Staring with an instantaneous slab source in an infinite one-dimensional reservoir (**Fig. 5**), overlaying three of such sources in x, y, and z direction makes a three-dimensional instantaneous slab source in a box-shaped reservoir. To obtain the solution of the new system, we multiple the three solutions of the original one-dimensional problem to have an instantaneous solution for the three-dimensional system. Integrate over the well trajectory or the fracture length and height to get the instantaneous slab source solution for the performance of the well, and then integrate over the time to get the three-dimension continuous slab source solution to solve practical reservoir problems. The procedure is summarized in **Fig. 6**. The solution as instantaneous source depends on the locations of the slab source and the box shape reservoir. To apply this method for horizontal wells with or without fractures, we define the source term (the

location and the dimensions of the source) and the main domain according to each individual physical system.

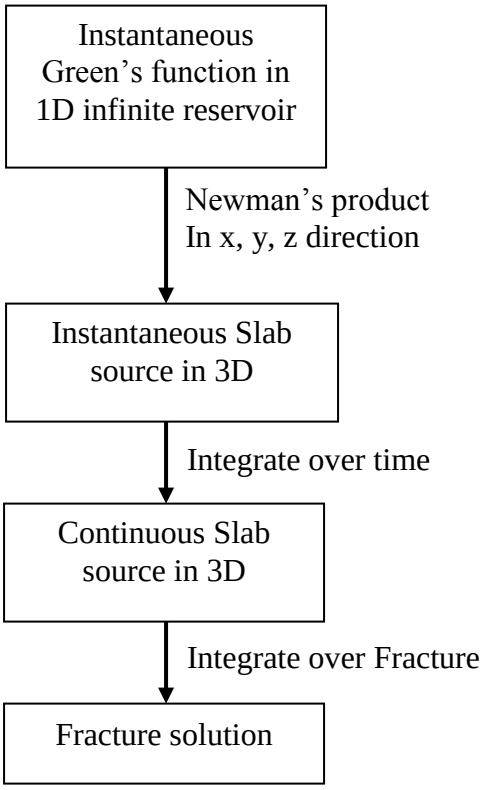

Fig. 6—Slab source solution flowchart.

For instance, the pressure drop as a results of a constant production, q, at a position (x_0,y_0,z_0) in an anisotropic box-shaped reservoir measured at a position (x, y, z) is readily calculate by

$$p_{\text{int}} - p(x,y,z,t) = \left[\frac{B\mu q}{abh\alpha}\right](s_x s_y s_z) \tag{2.8}$$

where, a is reservoir width, b is reservoir length, h is reservoir height, and s_x, s_y and s_z are the slab source functions in each direction depending on the boundary conditions, as shown in **Table 2**.

For no-flow boundary condition, and s_x, s_y, and s_z are

$$s_x = \frac{x_f}{a}\left[1+\frac{4a}{\pi x_f}\sum_{n=1}^{\infty}\frac{1}{n}\sin\frac{n\pi x_f}{2a}\cos\frac{n\pi x_o}{a}\cos\frac{n\pi x}{a}exp\left(-\frac{n^2\pi^2 k_x\tau}{a^2}\right)\right] \quad (2.9)$$

$$s_y = \frac{y_f}{b}\left[1+\frac{4b}{\pi y_f}\sum_{m=1}^{\infty}\frac{1}{m}\sin\frac{m\pi y_f}{2b}\cos\frac{m\pi y_o}{b}\cos\frac{m\pi y}{b}exp\left(-\frac{m^2\pi^2 k_y\tau}{b^2}\right)\right] \quad (2.10)$$

$$s_z = \frac{z_f}{b}\left[1+\frac{4h}{\pi z_f}\sum_{l=1}^{\infty}\frac{1}{l}\sin\frac{l\pi z_f}{2h}\cos\frac{l\pi z_o}{h}\cos\frac{l\pi z}{h}exp\left(-\frac{l^2\pi^2 k_z\tau}{h^2}\right)\right] \quad (2.11)$$

After obtain the instantaneous slab source solution under defined boundary conditions, we integrate the instantaneous point source over a time interval to attain the continuous slab source solution. The pressure drop at point (x, y, z) as a result of the continuous production or injection at position (x_0, y_0, z_0) in an anisotropic box-shaped reservoir then is

$$p_{\text{int}} - p(x,y,z,t) = \int_0^t\left[\frac{B_0\mu_0 q_0}{abh\alpha}\right](s_x s_y s_z)d\tau \quad (2.12)$$

For the slab source representing a fracture as shown in **Fig. 7**, the solution of the continuous slab source can be written as,

$$p_{\text{int}} - p(x,y,z,t) = \left[\frac{B_0\mu_0 q_0}{abh\alpha}\right]\int_{z_1}^{z_2}\int_{y_1}^{y_2}\int_{x_1}^{x_2}\int_0^t(s_x s_y s_z)d\tau dxdydz \quad (2.13)$$

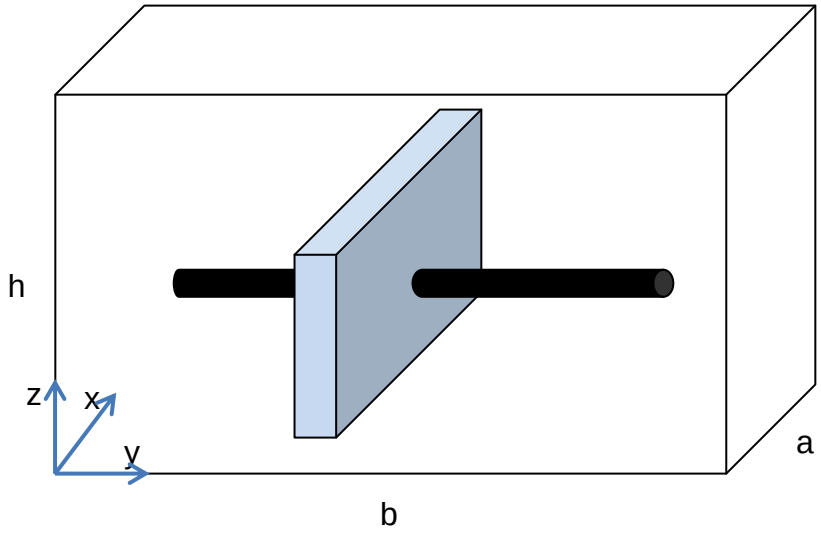

Fig. 7—Schematic of a single fracture.

To integrate Eq.(2.13), the solution is

$$p_{\text{int}} - p(x,y,z,t) = \left[\frac{B_o \mu_o q_o}{\alpha abh(x_2 - x_1)(y_2 - y_1)(z_2 - z_1)}\right] F(x,y,z,t) \qquad (2.14)$$

where F(x, y, z, t) is equal to

$$\mathrm{F(x,y,z,t)} = (\mathrm{x}_2 - x_1)(\mathrm{y}_2 - y_1)(\mathrm{z}_2 - z_1)t$$

$$+ \frac{4\alpha a^4 (\mathrm{y}_2 - y_1)(\mathrm{z}_2 - z_1)}{\pi^4 k_x x_f} \sum_{n=1}^{\infty} \frac{1}{n^4} \cos\frac{n\pi x}{a} \sin\frac{n\pi x_f}{2a}$$

$$* \left(\sin\frac{n\pi x_2}{a} - \sin\frac{n\pi x_1}{a}\right)\left[1 - \exp\left(-\frac{n^2\pi^2 k_x t}{\alpha a^2}\right)\right]$$

$$+ \frac{4\alpha b^4 (\mathrm{x}_2 - x_1)(\mathrm{z}_2 - z_1)}{\pi^4 k_y y_f} \sum_{m=1}^{\infty} \frac{1}{m^4} \cos\frac{m\pi y}{b} \sin\frac{m\pi y_f}{2b}$$

$$*\left(\sin\frac{m\pi y_2}{b}-\sin\frac{m\pi y_1}{b}\right)\left[1-\exp\left(-\frac{m^2\pi^2 k_x t}{\alpha b^2}\right)\right]$$

$$+\frac{4\alpha h^4\left(\mathrm{x}_2-x_1\right)\left(\mathrm{y}_2-y_1\right)}{\pi^4 k_z z_f}\sum_{l=1}^{\infty}\frac{1}{l^4}\cos\frac{l\pi z}{h}\sin\frac{n\pi z_f}{2h}$$

$$*\left(\sin\frac{l\pi z_2}{h}-\sin\frac{l\pi z_1}{h}\right)\left[1-\exp\left(-\frac{l^2\pi^2 k_z t}{\alpha h^2}\right)\right]$$

$$+\frac{16\alpha a^2 b^2\left(\mathrm{z}_2-z_1\right)}{\pi^6 x_f y_f}\sum_{m=1}^{\infty}\sum_{n=1}^{\infty}\left(\sin\frac{n\pi x_2}{a}-\sin\frac{n\pi x_1}{a}\right)\left(\sin\frac{m\pi y_2}{b}-\sin\frac{m\pi y_1}{b}\right)$$

$$*\frac{\sin\frac{n\pi x_f}{2a}\cos\frac{n\pi x}{a}\sin\frac{m\pi y_2}{2b}\sin\frac{m\pi x}{b}}{n^2m^2\left(\frac{n^2k_x}{a^2}+\frac{m^2k_y}{b^2}\right)}\left\{1-\exp\left[-\frac{\pi^2 t}{\alpha}\left(\frac{n^2k_x}{a^2}+\frac{m^2k_y}{b^2}\right)\right]\right\}$$

$$+\frac{16\alpha a^2 h^2\left(\mathrm{y}_2-y_1\right)}{\pi^6 x_f z_f}\sum_{n=1}^{\infty}\sum_{l=1}^{\infty}\left(\sin\frac{n\pi x_2}{a}-\sin\frac{n\pi x_1}{a}\right)\left(\sin\frac{l\pi z_2}{h}-\sin\frac{l\pi z_1}{h}\right)$$

$$*\frac{\sin\frac{n\pi x_f}{2a}\cos\frac{n\pi x}{a}\sin\frac{l\pi z_2}{2h}\sin\frac{l\pi z}{h}}{n^2l^2\left(\frac{n^2k_x}{a^2}+\frac{l^2k_z}{h^2}\right)}\left\{1-\exp\left[-\frac{\pi^2 t}{\alpha}\left(\frac{n^2k_x}{a^2}+\frac{l^2k_z}{h^2}\right)\right]\right\}$$

$$+\frac{16\alpha b^2 h^2\left(\mathrm{x}_2-x_1\right)}{\pi^6 y_f z_f}\sum_{m=1}^{\infty}\sum_{l=1}^{\infty}\left(\sin\frac{m\pi y_2}{b}-\sin\frac{m\pi y_1}{b}\right)\left(\sin\frac{l\pi z_2}{h}-\sin\frac{l\pi z_1}{h}\right)$$

$$*\frac{\sin\frac{m\pi y_f}{2b}\cos\frac{m\pi y}{b}\sin\frac{l\pi z_2}{2h}\sin\frac{l\pi z}{h}}{m^2l^2\left(\frac{m^2k_y}{b^2}+\frac{l^2k_z}{h^2}\right)}\left\{1-\exp\left[-\frac{\pi^2 t}{\alpha}\left(\frac{m^2k_y}{b^2}+\frac{l^2k_z}{h^2}\right)\right]\right\}$$

$$+\frac{64\alpha a^2 b^2 h^2}{\pi^8 x_f y_f z_f}\sum_{n=1}^{\infty}\sum_{m=1}^{\infty}\sum_{l=1}^{\infty}\left(\sin\frac{n\pi x_2}{a}-\sin\frac{n\pi x_1}{a}\right)\left(\sin\frac{m\pi y_2}{b}-\sin\frac{m\pi y_1}{b}\right)$$

$$*\left(\sin\frac{l\pi z_2}{h}-\sin\frac{l\pi z_1}{h}\right)\left\{1-\exp\left[-\frac{\pi^2 t}{\alpha}\left(\frac{n^2k_x}{a^2}+\frac{m^2k_y}{b^2}+\frac{l^2k_z}{h^2}\right)\right]\right\}$$

$$*\frac{\sin\frac{n\pi x_f}{2a}\cos\frac{n\pi z}{a}\sin\frac{m\pi y_f}{2b}\cos\frac{m\pi y}{b}\sin\frac{l\pi z_2}{2h}\sin\frac{l\pi z}{h}}{n^2m^2l^2\left(\frac{n^2k_x}{a^2}+\frac{m^2k_y}{b^2}+\frac{l^2k_z}{h^2}\right)} \qquad (2.15)$$

At late time or stabilized flow, the exponential terms in Eq. (2.15) becomes zero and it reduced to

$$p_{\text{int}}-p(x,y,z,t)=\left[\frac{B_o\mu_o q_o}{\alpha abh(x_2-x_1)(y_2-y_1)(z_2-z_1)}\right]$$

$$\{(x_2-x_1)(y_2-y_1)(z_2-z_1)t$$

$$+\frac{4\alpha a^4(y_2-y_1)(z_2-z_1)}{\pi^4k_xx_f}\sum_{n=1}^{\infty}\frac{1}{n^4}\cos\frac{n\pi x}{a}\sin\frac{n\pi x_f}{2a}\left(\sin\frac{n\pi x_2}{a}-\sin\frac{n\pi x_1}{a}\right)$$

$$+\frac{4\alpha b^4(x_2-x_1)(z_2-z_1)}{\pi^4k_yy_f}\sum_{m=1}^{\infty}\frac{1}{m^4}\cos\frac{m\pi y}{b}\sin\frac{m\pi y_f}{2b}\left(\sin\frac{m\pi y_2}{b}-\sin\frac{m\pi y_1}{b}\right)$$

$$+\frac{4\alpha h^4(x_2-x_1)(y_2-y_1)}{\pi^4k_zz_f}\sum_{l=1}^{\infty}\frac{1}{l^4}\cos\frac{l\pi z}{h}\sin\frac{n\pi z_f}{2h}\left(\sin\frac{l\pi z_2}{h}-\sin\frac{l\pi z_1}{h}\right)$$

$$+\frac{16\alpha a^2b^2(z_2-z_1)}{\pi^6x_fy_f}\sum_{m=1}^{\infty}\sum_{n=1}^{\infty}\left(\sin\frac{n\pi x_2}{a}-\sin\frac{n\pi x_1}{a}\right)\left(\sin\frac{m\pi y_2}{b}-\sin\frac{m\pi y_1}{b}\right)$$

$$*\frac{\sin\frac{n\pi x_f}{2a}\cos\frac{n\pi x}{a}\sin\frac{m\pi y_2}{2b}\sin\frac{m\pi x}{b}}{n^2m^2\left(\frac{n^2k_x}{a^2}+\frac{m^2k_y}{b^2}\right)}$$

$$+\frac{16\alpha a^2h^2\left(y_2-y_1\right)}{\pi^6x_fz_f}\sum_{n=1}^{\infty}\sum_{l=1}^{\infty}\left(\sin\frac{n\pi x_2}{a}-\sin\frac{n\pi x_1}{a}\right)\left(\sin\frac{l\pi z_2}{h}-\sin\frac{l\pi z_1}{h}\right)$$

$$*\frac{\sin\frac{n\pi x_f}{2a}\cos\frac{n\pi x}{a}\sin\frac{l\pi z_2}{2h}\sin\frac{l\pi z}{h}}{n^2l^2\left(\frac{n^2k_x}{a^2}+\frac{l^2k_z}{h^2}\right)}$$

$$+\frac{16\alpha b^2h^2\left(x_2-x_1\right)}{\pi^6y_fz_f}\sum_{m=1}^{\infty}\sum_{l=1}^{\infty}\left(\sin\frac{m\pi y_2}{b}-\sin\frac{m\pi y_1}{b}\right)\left(\sin\frac{l\pi z_2}{h}-\sin\frac{l\pi z_1}{h}\right)$$

$$*\frac{\sin\frac{m\pi y_f}{2b}\cos\frac{m\pi y}{b}\sin\frac{l\pi z_2}{2h}\sin\frac{l\pi z}{h}}{m^2l^2\left(\frac{m^2k_y}{b^2}+\frac{l^2k_z}{h^2}\right)}$$

$$+\frac{64\alpha a^2b^2h^2}{\pi^8x_fy_fz_f}\sum_{n=1}^{\infty}\sum_{m=1}^{\infty}\sum_{l=1}^{\infty}\left(\sin\frac{n\pi x_2}{a}-\sin\frac{n\pi x_1}{a}\right)\left(\sin\frac{m\pi y_2}{b}-\sin\frac{m\pi y_1}{b}\right)$$

$$*\left(\sin\frac{l\pi z_2}{h}-\sin\frac{l\pi z_1}{h}\right)\left\{\frac{\sin\frac{n\pi x_f}{2a}\cos\frac{n\pi z}{a}\sin\frac{m\pi y_f}{2b}\cos\frac{m\pi y}{b}\sin\frac{l\pi z_2}{2h}\sin\frac{l\pi z}{h}}{n^2m^2l^2\left(\frac{n^2k_x}{a^2}+\frac{m^2k_y}{b^2}+\frac{l^2k_z}{h^2}\right)}\right\}$$

(2.16)

For stabilized flow under pseudo-steady-state condition, the average reservoir pressure can be written as

$$p_{\text{int}}-\bar{p}=\frac{B_oN_p}{V_pc_t} \tag{2.17}$$

Defining the drainage volume, then

$$p_{\text{int}} = \bar{p} + \frac{B_o q_o}{abh\phi c_t} t \tag{2.18}$$

Because $\alpha = \phi\mu c_t$ we substitute α into Eq. (2.18) and we obtain

$$p_{\text{int}} = \bar{p} + \frac{\mu_o B_o q_o}{abh\alpha} t \tag{2.19}$$

Substituting Eq. (2.19) into Eq.(2.17), we have

$$\bar{p} - p(x,y,z,t) = \left[\frac{B_o \mu_o q_o}{\alpha abh}\right]\left\{\frac{4\alpha a^4}{(x_2 - x_1)\pi^4 k_x x_f}\right.$$

$$* \sum_{n=1}^{\infty} \frac{1}{n^4} \cos\frac{n\pi x}{a} \sin\frac{n\pi x_f}{2a}\left(\sin\frac{n\pi x_2}{a} - \sin\frac{n\pi x_1}{a}\right)$$

$$+ \frac{4\alpha b^4}{(y_2 - y_1)\pi^4 k_y y_f} \sum_{m=1}^{\infty} \frac{1}{m^4} \cos\frac{m\pi y}{b}\left(\sin\frac{m\pi y_2}{b} - \sin\frac{m\pi y_1}{b}\right)\sin\frac{m\pi y_f}{2b}$$

$$+ \frac{4\alpha h^4}{(z_2 - z_1)\pi^4 k_z z_f} \sum_{l=1}^{\infty} \frac{1}{l^4} \cos\frac{l\pi z}{h} \sin\frac{n\pi z_f}{2h}\left(\sin\frac{l\pi z_2}{h} - \sin\frac{l\pi z_1}{h}\right)$$

$$+ \frac{16\alpha a^2 b^2}{\pi^6 x_f y_f (x_2 - x_1) y (z_2 - y_1)} \sum_{m=1}^{\infty}\sum_{n=1}^{\infty}\left(\sin\frac{n\pi x_2}{a} - \sin\frac{n\pi x_1}{a}\right)$$

$$* \left(\sin\frac{m\pi y_2}{b} - \sin\frac{m\pi y_1}{b}\right) \frac{\sin\dfrac{n\pi x_f}{2a} \cos\dfrac{n\pi x}{a} \sin\dfrac{m\pi y_2}{2b} \sin\dfrac{m\pi x}{b}}{n^2 m^2 \left(\dfrac{n^2 k_x}{a^2} + \dfrac{m^2 k_y}{b^2}\right)}$$

$$+ \frac{16\alpha a^2 h^2}{\pi^6 x_f z_f (x_2 - x_1)(z_2 - z_1)} \sum_{n=1}^{\infty}\sum_{l=1}^{\infty}\left(\sin\frac{n\pi x_2}{a} - \sin\frac{n\pi x_1}{a}\right)$$

$$*\left(\sin\frac{l\pi z_2}{h}-\sin\frac{l\pi z_1}{h}\right)\frac{\sin\frac{n\pi x_f}{2a}\cos\frac{n\pi x}{a}\sin\frac{l\pi z_2}{2h}\sin\frac{l\pi z}{h}}{n^2l^2\left(\frac{n^2k_x}{a^2}+\frac{l^2k_z}{h^2}\right)}$$

$$+\frac{16\alpha b^2h^2}{\pi^6 y_f z_f (y_2-y_1)(z_2-z_1)}\sum_{m=1}^{\infty}\sum_{l=1}^{\infty}\left(\sin\frac{m\pi y_2}{b}-\sin\frac{m\pi y_1}{b}\right)$$

$$*\left(\sin\frac{l\pi z_2}{h}-\sin\frac{l\pi z_1}{h}\right)\frac{\sin\frac{m\pi y_f}{2b}\cos\frac{m\pi y}{b}\sin\frac{l\pi z_2}{2h}\sin\frac{l\pi z}{h}}{m^2l^2\left(\frac{m^2k_y}{b^2}+\frac{l^2k_z}{h^2}\right)}$$

$$+\frac{64\alpha a^2b^2h^2}{\pi^8 x_f y_f z_f (x_2-x_1)(y_2-y_1)(z_2-z_1)}\sum_{n=1}^{\infty}\sum_{m=1}^{\infty}\sum_{l=1}^{\infty}\left(\sin\frac{n\pi x_2}{a}-\sin\frac{n\pi x_1}{a}\right)$$

$$*\left(\sin\frac{m\pi y_2}{b}-\sin\frac{m\pi y_1}{b}\right)\left(\sin\frac{l\pi z_2}{h}-\sin\frac{l\pi z_1}{h}\right)$$

$$*\frac{\sin\frac{n\pi x_f}{2a}\cos\frac{n\pi z}{a}\sin\frac{m\pi y_f}{2b}\cos\frac{m\pi y}{b}\sin\frac{l\pi z_2}{2h}\sin\frac{l\pi z}{h}}{n^2m^2l^2\left(\frac{n^2k_x}{a^2}+\frac{m^2k_y}{b^2}+\frac{l^2k_z}{h^2}\right)}\Bigg\} \tag{2.20}$$

In oil field unit, Eq. (2.20) becomes

$$\bar{p}-p(x,y,z,t)=\left[\frac{887.53B_o\mu_o q_o}{\alpha abh}\right]\Bigg\{\frac{4\alpha a^4}{(x_2-x_1)\pi^4 k_x x_f}$$

$$*\sum_{n=1}^{\infty}\frac{1}{n^4}\cos\frac{n\pi x}{a}\sin\frac{n\pi x_f}{2a}\left(\sin\frac{n\pi x_2}{a}-\sin\frac{n\pi x_1}{a}\right)$$

$$+\frac{4\alpha b^4}{(y_2-y_1)\pi^4 k_y y_f}\sum_{m=1}^{\infty}\frac{1}{m^4}\cos\frac{m\pi y}{b}\left(\sin\frac{m\pi y_2}{b}-\sin\frac{m\pi y_1}{b}\right)\sin\frac{m\pi y_f}{2b}$$

$$+\frac{4\alpha h^4}{(z_2-z_1)\pi^4 k_z z_f}\sum_{l=1}^{\infty}\frac{1}{l^4}\cos\frac{l\pi z}{h}\sin\frac{n\pi z_f}{2h}\left(\sin\frac{l\pi z_2}{h}-\sin\frac{l\pi z_1}{h}\right)$$

$$+\frac{16\alpha a^2 b^2}{\pi^6 x_f y_f (x_2-x_1) y (z_2-y_1)}\sum_{m=1}^{\infty}\sum_{n=1}^{\infty}\left(\sin\frac{n\pi x_2}{a}-\sin\frac{n\pi x_1}{a}\right)$$

$$*\left(\sin\frac{m\pi y_2}{b}-\sin\frac{m\pi y_1}{b}\right)\frac{\sin\frac{n\pi x_f}{2a}\cos\frac{n\pi x}{a}\sin\frac{m\pi y_2}{2b}\sin\frac{m\pi x}{b}}{n^2 m^2\left(\frac{n^2 k_x}{a^2}+\frac{m^2 k_y}{b^2}\right)}$$

$$+\frac{16\alpha a^2 h^2}{\pi^6 x_f z_f (x_2-x_1)(z_2-z_1)}\sum_{n=1}^{\infty}\sum_{l=1}^{\infty}\left(\sin\frac{n\pi x_2}{a}-\sin\frac{n\pi x_1}{a}\right)$$

$$*\left(\sin\frac{l\pi z_2}{h}-\sin\frac{l\pi z_1}{h}\right)\frac{\sin\frac{n\pi x_f}{2a}\cos\frac{n\pi x}{a}\sin\frac{l\pi z_2}{2h}\sin\frac{l\pi z}{h}}{n^2 l^2\left(\frac{n^2 k_x}{a^2}+\frac{l^2 k_z}{h^2}\right)}$$

$$+\frac{16\alpha b^2 h^2}{\pi^6 y_f z_f (y_2-y_1)(z_2-z_1)}\sum_{m=1}^{\infty}\sum_{l=1}^{\infty}\left(\sin\frac{m\pi y_2}{b}-\sin\frac{m\pi y_1}{b}\right)$$

$$*\left(\sin\frac{l\pi z_2}{h}-\sin\frac{l\pi z_1}{h}\right)\frac{\sin\frac{m\pi y_f}{2b}\cos\frac{m\pi y}{b}\sin\frac{l\pi z_2}{2h}\sin\frac{l\pi z}{h}}{m^2 l^2\left(\frac{m^2 k_y}{b^2}+\frac{l^2 k_z}{h^2}\right)}$$

$$+\frac{64\alpha a^2 b^2 h^2}{\pi^8 x_f y_f z_f (x_2-x_1)(y_2-y_1)(z_2-z_1)}$$

$$\left.\frac{\sin\frac{n\pi x_f}{2a}\cos\frac{n\pi z}{a}\sin\frac{m\pi y_f}{2b}\cos\frac{m\pi y}{b}\sin\frac{l\pi z_2}{2h}\sin\frac{l\pi z}{h}}{n^2m^2l^2\left(\frac{n^2k_x}{a^2}+\frac{m^2k_y}{b^2}+\frac{l^2k_z}{h^2}\right)}\right\} \tag{2.21}$$

where $\alpha = 158.73\phi\mu c_t$

For gas reservoir, Eq.(2.20) becomes

$$\bar{p}^2 - p(x,y,z,t)^2 = \left[\frac{8947\mu q_o ZT}{\alpha abh}\right]\left\{\frac{4\alpha a^4}{(x_2-x_1)\pi^4 k_x x_f}\right.$$

$$*\sum_{n=1}^{\infty}\frac{1}{n^4}\cos\frac{n\pi x}{a}\sin\frac{n\pi x_f}{2a}\left(\sin\frac{n\pi x_2}{a}-\sin\frac{n\pi x_1}{a}\right)$$

$$+\frac{4\alpha b^4}{(y_2-y_1)\pi^4 k_y y_f}\sum_{m=1}^{\infty}\frac{1}{m^4}\cos\frac{m\pi y}{b}\left(\sin\frac{m\pi y_2}{b}-\sin\frac{m\pi y_1}{b}\right)\sin\frac{m\pi y_f}{2b}$$

$$+\frac{4\alpha h^4}{(z_2-z_1)\pi^4 k_z z_f}\sum_{l=1}^{\infty}\frac{1}{l^4}\cos\frac{l\pi z}{h}\sin\frac{n\pi z_f}{2h}\left(\sin\frac{l\pi z_2}{h}-\sin\frac{l\pi z_1}{h}\right)$$

$$+\frac{16\alpha a^2 b^2}{\pi^6 x_f y_f (x_2-x_1) y (z_2-y_1)}\sum_{m=1}^{\infty}\sum_{n=1}^{\infty}\left(\sin\frac{n\pi x_2}{a}-\sin\frac{n\pi x_1}{a}\right)$$

$$*\left(\sin\frac{m\pi y_2}{b}-\sin\frac{m\pi y_1}{b}\right)\frac{\sin\frac{n\pi x_f}{2a}\cos\frac{n\pi x}{a}\sin\frac{m\pi y_2}{2b}\sin\frac{m\pi x}{b}}{n^2m^2\left(\frac{n^2k_x}{a^2}+\frac{m^2k_y}{b^2}\right)}$$

$$+\frac{16\alpha a^2 h^2}{\pi^6 x_f z_f (x_2-x_1)(z_2-z_1)}\sum_{n=1}^{\infty}\sum_{l=1}^{\infty}\left(\sin\frac{n\pi x_2}{a}-\sin\frac{n\pi x_1}{a}\right)$$

$$*\left(\sin\frac{l\pi z_2}{h}-\sin\frac{l\pi z_1}{h}\right)\frac{\sin\frac{n\pi x_f}{2a}\cos\frac{n\pi x}{a}\sin\frac{l\pi z_2}{2h}\sin\frac{l\pi z}{h}}{n^2l^2\left(\frac{n^2k_x}{a^2}+\frac{l^2k_z}{h^2}\right)}$$

$$+\frac{16\alpha b^2h^2}{\pi^6 y_f z_f (y_2-y_1)(z_2-z_1)}\sum_{m=1}^{\infty}\sum_{l=1}^{\infty}\left(\sin\frac{m\pi y_2}{b}-\sin\frac{m\pi y_1}{b}\right)$$

$$*\left(\sin\frac{l\pi z_2}{h}-\sin\frac{l\pi z_1}{h}\right)\frac{\sin\frac{m\pi y_f}{2b}\cos\frac{m\pi y}{b}\sin\frac{l\pi z_2}{2h}\sin\frac{l\pi z}{h}}{m^2l^2\left(\frac{m^2k_y}{b^2}+\frac{l^2k_z}{h^2}\right)}$$

$$+\frac{64\alpha a^2b^2h^2}{\pi^8 x_f y_f z_f (x_2-x_1)(y_2-y_1)(z_2-z_1)}\sum_{n=1}^{\infty}\sum_{m=1}^{\infty}\sum_{l=1}^{\infty}\left(\sin\frac{n\pi x_2}{a}-\sin\frac{n\pi x_1}{a}\right)$$

$$\left(\sin\frac{m\pi y_2}{b}-\sin\frac{m\pi y_1}{b}\right)\left(\sin\frac{l\pi z_2}{h}-\sin\frac{l\pi z_1}{h}\right)$$

$$\left.\frac{\sin\frac{n\pi x_f}{2a}\cos\frac{n\pi z}{a}\sin\frac{m\pi y_f}{2b}\cos\frac{m\pi y}{b}\sin\frac{l\pi z_2}{2h}\sin\frac{l\pi z}{h}}{n^2m^2l^2\left(\frac{n^2k_x}{a^2}+\frac{m^2k_y}{b^2}+\frac{l^2k_z}{h^2}\right)}\right\} \qquad (2.22)$$

2.1.4 Horizontal Well in Slab Source Solution

Using the slab source solution to calculate a horizontal well without fractures performance, first define inner boundary condition, then to count pressure change inside a wellbore, we divide the wellbore into N segments. Each segment connects to each other by superpositioning in space. By using this technique, a set of linear equation is

generated and the solution of the system equation predicts the well performance. For horizontal well showed in **Fig. 8**, the pressure drop causes by a constant production flow rate, q_1, into segment 1 is evaluated on the well circumstance are the middle of every well segment. For each segment, we have a set of N linear equations for pressure respond to the flow. With N segments, there are N set of N linear equations as shown in Eq. (2.24).

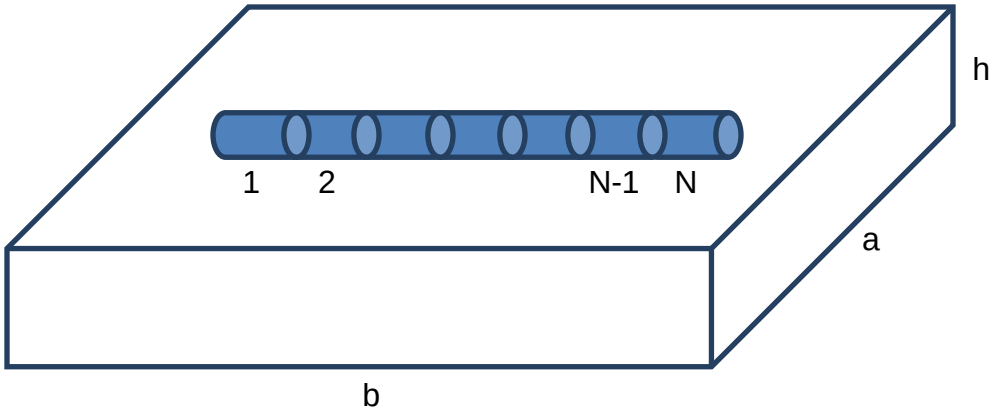

Fig. 8—Schematic of slab source for horizontal well.

$$q_1F(1,1)+q_2F(1,2)+q_3F(1,3)+\ldots+q_NF(1,N)=\Delta p_1$$

$$q_1F(2,1)+q_2F(2,2)+q_3F(2,3)+\ldots+q_NF(2,N)=\Delta p_2$$

$$q_1F(3,1)+q_2F(3,2)+q_3F(3,3)+\ldots+q_NF(3,N)=\Delta p_3$$

.
.
.

$$q_1 F(N,1) + q_2 F(N,2) + q_3 F(N,3) + ... + q_N F(N,N) = \Delta p_N \qquad (2.23)$$

2.1.5 Fracture System in Slab Source Solution

For fractures, we divided each fracture into N*N segments, each segment will create flow rate from the reservoir. For example, we have a fracture with 25 segments as shown in **Fig. 9**, each segment is contact with each other. To simplify the problem, it is assumed that in such a system, only fracture create flow rate. Similar to the horizontal well system, each segment will generate flow rate from the reservoir. Because of the flow rate in the segment 1, the pressure for the other 24 segment will be changed. By the same way, the flow rate of the second segment would change the pressure distribution in the other 24 segments. With N*N segments, we have a set of N*N linear equations for pressure respond to the flow in the fracture. The horizontal well takes flow rate from the fracture, but not directly from the reservoir.

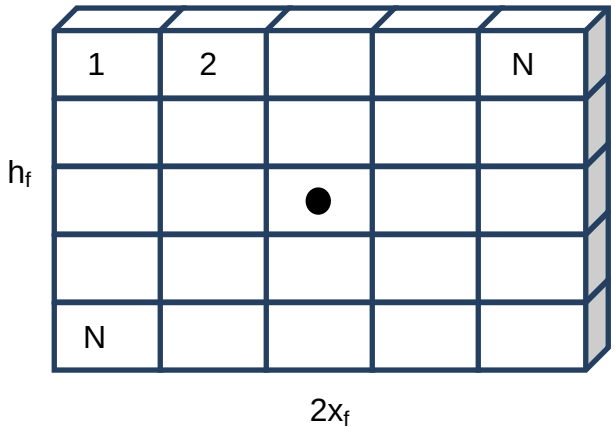

Fig. 9—Discretized fracture.

The pressure drop as a result of each fracture segment produces at a constant rate is calculated by Eq. (2.14). The pressure at segment **i** as a result of the production, q_j, at segment **j** is evaluated by multiplying q_j with F(i,j) as shown in Eq. (2.14) and (2.15). For the entire fracture (N segment), we obtain a set of linear equation shown as,

$$q_1F(1,1)+q_2F(1,2)+q_3F(1,3)+...+q_NF(1,N)=\Delta p_1$$

$$q_1F(2,1)+q_2F(2,2)+q_3F(2,3)+...+q_NF(2,N)=\Delta p_2$$

$$q_1F(3,1)+q_2F(3,2)+q_3F(3,3)+...+q_NF(3,N)=\Delta p_3$$

.
.
.

$$q_1F(N,1)+q_2F(N,2)+q_3F(N,3)+...+q_NF(N,N)=\Delta p_N \qquad (2.24)$$

where, q_j is a constant flow rate flow into segment j and Δp_j is the pressure drop calculated at segment j as a result of the production into every segment. The total production from the fracture is calculated by

$$\sum_{j=1}^{n} q_j = q_{total} \qquad (2.25)$$

where q_{total} is the total production for every segment, or the maximum flow rate if the well constraint is constant production rate. By using the above method, we can calculate the horizontal well with fractures performance in uniform flux boundary condition, infinite boundary condition, and finite boundary condition. The well system is predicted by either a constant flow rate constraint or constant wellbore pressure constraint.

The inflow distribution along the wellbore or fracture depends on the inner boundary conditions.

2.1.6 Solution for Infinite Conductivity Condition

In infinite conductivity condition for fractures, we divided the source into N segments. For a source under infinite conductivity, uniform pressure over the source is assumed.

Fig. 9 shows an example of how the source is discretized into 25 segments. For the infinite conductivity inner boundary condition, the wellbore pressure is constant along the well or the fracture. The right hand side in Eq. (2.26) have the same pressure drop which shown in Eq. (2.27).In this way, we could solve the set of liner equations and get the flow rate along the fracture.

$$q_1F(1,1)+q_2F(1,2)+q_3F(1,3)+...+q_{25}F(1,25)=p_i-p_1$$

$$q_1F(2,1)+q_2F(2,2)+q_3F(2,3)+...+q_{25}F(2,25)=p_i-p_2$$

$$q_1F(3,1)+q_2F(3,2)+q_3F(3,3)+...+q_{25}F(3,25)=p_i-p_3$$

.
.
.

$$q_1F(25,1)+q_2F(25,2)+q_3F(25,3)+...+q_{25}F(25,25)=p_i-p_{25} \quad (2.26)$$

$$p_i=p_2=...=p_{25} \quad (2.27)$$

2.1.7 Solution for Finite Conductivity Condition

For the cases with finite conductivity we use the same approach as the infinite conductivity except we have to introduce another term to account for the pressure drop between source segments because of the source conductivity.

We first define the inner boundary condition at the interface of the source and the domain (for example, the wellbore and the reservoir). Then we divide the fracture into multiple segments. The segments are then connected to each other by super position in the space. By using this technique, a set of linear equation is generated and solved to predict the fractured horizontal well performance. **Fig. 10** shows an example for 25 sources fracture. We first allow source 1 to exist in the reservoir and let it generate a flow rate of q_1 at the location. The flow results in corresponding pressure changes at locations of sources 2 through 25. Then if we only let source 2 exists the pressure also changes at all source locations. We can apply this procedure to all 25 sources in the system. To illustrate the influence of the source location, we use dimensional format of the equations in this section.

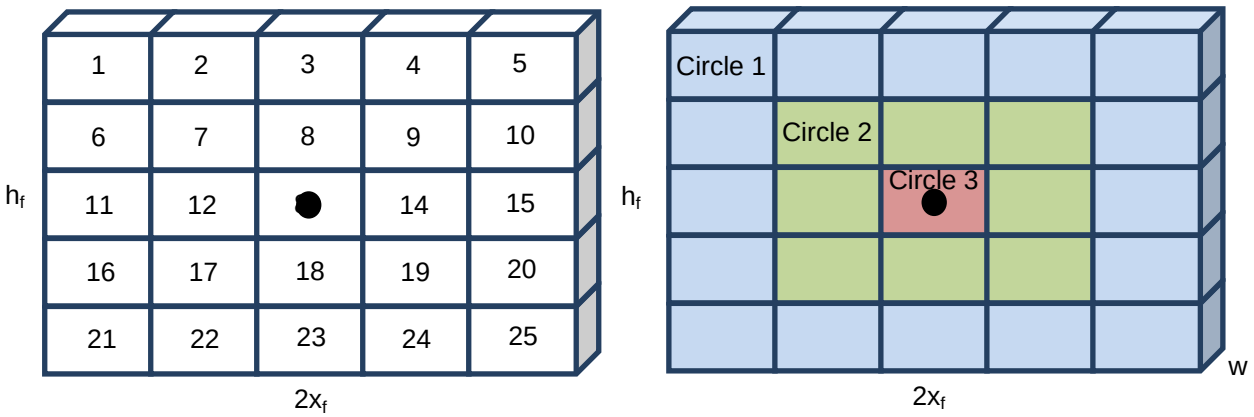

Fig. 10—Segment fracture for finite conductivity.

An additional pressure drop will be added to the calculation, which is showed in **Fig. 10**. Three circles are defined in the fracture. Circle 1 is in blue, circle 2 is in green and

circle 3 is in pink. The fluid will firstly flow from the out boundary to inner boundary of circle 1(seg. 1-5, 6, 10-11, 15-16, and 20-25). Then the fluid flows inside circle 2(seg. 7-9, 12, 14, 17-19). Finally it flows from circle 3 to wellbore. In such a way, we could easily calculate the pressure drop inside of the fracture by Eq. (2.28).

$$\bar{p} - p_{wf} = \frac{141.2B\mu}{kh}\left(\frac{1}{2}\ln\frac{4A}{\gamma C_A r_w^2} + s\right)q \qquad (2.28)$$

where, A is drainage area, C_A is shape facture, and γ is Euler's constant.

The Earlougher's shape factor is shown in **Table 3**.

Table 3—Shape factor (Earlougher, 1977).

Drainage Area	Earlougher Shaper Factor
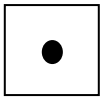	30.9
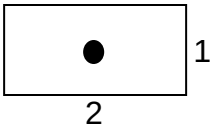	21.8
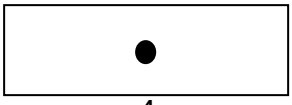	5.38
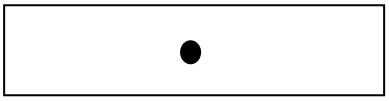	2.36

The procedures for calculating the flow rate and pressure drop along the fractures have two parts. One is from the reservoir to the fracture. The other is inside of the fractures. An example used here for a transverse fracture with 25 segments.

First it is the reservoir to fracture system. The fracture is divided into 25 segments. We start from the first segment to the last segment. The segment 1 will generate the flow rate from the reservoir, q_1, flowing into the fracture by using Eq. (2.22). After this calculation, we will have 25 F(1, j) terms. Then we move to the next segment which is segment 2 and repeat the same procedure but for this segment we evaluate the pressure drop as a result of a constant flow, q_2, flowing into segment 2 which gives another 25 F(2, j). We use the superposition principle in space to get a set of linear equation. The series of linear equation can be written as Eq. (2.29)

$$\begin{bmatrix} p_{\text{int}} \\ p_{\text{int}} \\ p_{\text{int}} \\ . \\ . \\ . \\ p_{\text{int}} \end{bmatrix} - \begin{bmatrix} p_1 \\ p_2 \\ p_3 \\ . \\ . \\ . \\ p_{25} \end{bmatrix} = \begin{bmatrix} F_{(1,1)}, F_{(1,2)} \ldots F_{(1,25)} \\ F_{(2,1)}, F_{(2,2)} \ldots F_{(2,25)} \\ F_{(3,1)}, F_{(3,2)} \ldots F_{(3,25)} \\ . \\ . \\ . \\ F_{(25,1)}, F_{(25,2)} \ldots F_{(25,25)} \end{bmatrix} \begin{bmatrix} q_1 \\ q_2 \\ q_3 \\ . \\ . \\ . \\ q_{25} \end{bmatrix} \tag{2.29}$$

Then, fluid inside fracture is analyzed. As shown in **Fig. 10**, for circle 1, the pressure drop in these segments could be calculated by Eq. (2.28). We rewrite the equation as the following

$$p_{i,circle1} - p_{inner,circle1} = Bq_{circle1} \tag{2.30}$$

p_i is the pressure at the middle point of each segment.

In the circle 2, the fluid flows from the out boundary of circle 2 to the middle of the segment, then to the inner boundary of circle 2. The flow rate will be the fluid flow inside of the segment plus the fluid comes from the circle 1.

$$p_{i,cicle2} - p_{inner,circle2} = Cq_{circle2} \tag{2.31}$$

$$p_{out,cirlce2} - p_{i,circle2} = Eq_{circle2} \tag{2.32}$$

Finally the fluid flows inside circle 3 from out boundary of circle 3 to the wellbore, it could be written as

$$p_{out,circle3} - p_{wf} = Dq_{circle3} \tag{2.33}$$

where, p_{wf} is the wellbore pressure.

To solve these equations, subsisting Eqs. (2.30), (2.31), Eq. (2.33) into Eq. (2.29) yields

$$p_{\text{int}} - p_{inner,circle1} - p_{inner,circle2} - p_{out,circle3} = (A + B + C - D)q_i \tag{2.34}$$

Adding Eq. (2.31) and Eq. (2.32)

$$p_{out,circle2} - p_{inner,circle2} = (E + C)q_i \tag{2.35}$$

where B, C, D, and E are the left part of Eq.(2.18) with different r_w, C_A, and A.

We also set that

$$p_{out,circle3} = p_{inner,circle2} \tag{2.36}$$

and

$$p_{out,circle2} = p_{inner,circle1} \tag{2.37}$$

The procedure to calculate the production and pressure distribution is showed in **Fig. 11**. We first assume the values of $p_{inner,circle1}$ and $p_{inner,circle2}$ to calculate the gas flow rate, and then calculate the $p_{out,circle2}$ by using Eq. (2.35).

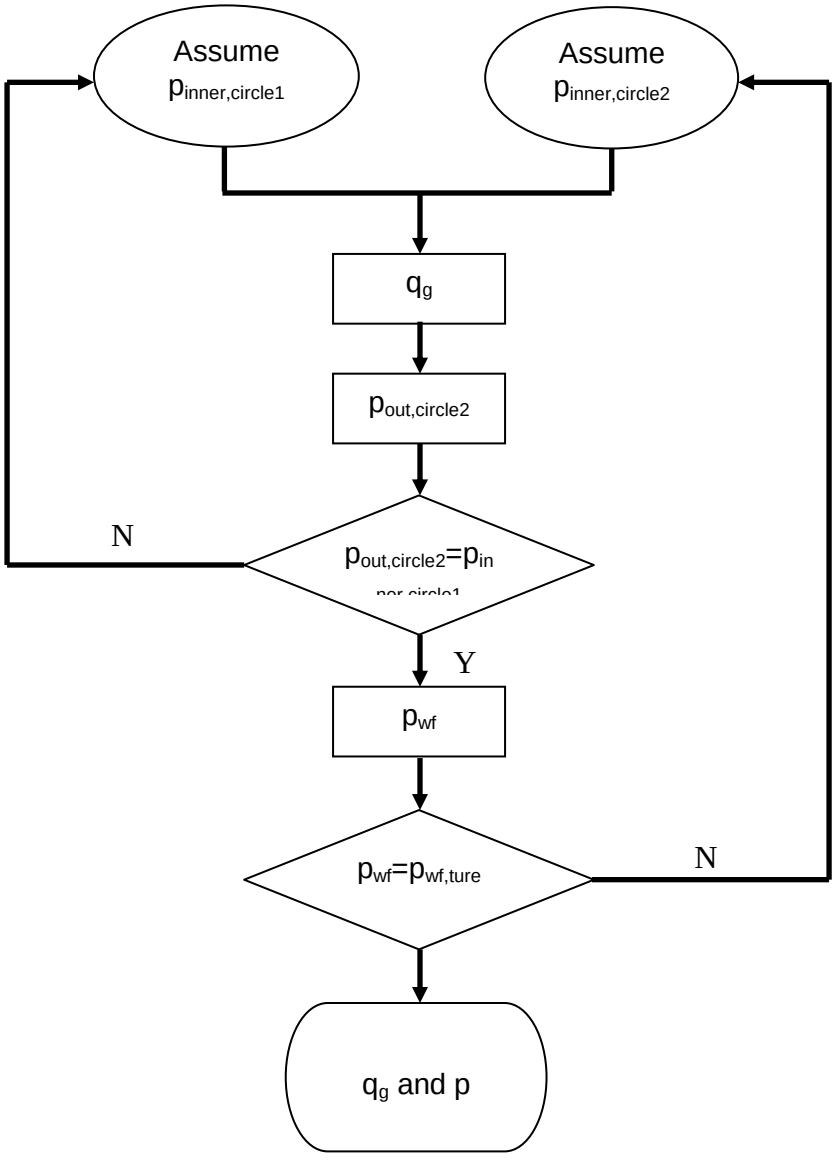

Fig. 11—Flow chart for pressure drop inside fracture.

We compared the $p_{out,circle2}$ and $p_{inner,circle1}$ to check whether they are the same. If it is not, we will set a new $p_{inner,circle1}$ value which is equal to $p_{out,2}$ to iterate until $p_{out,cirlce2}$ is equal to $p_{inner,circle1}$. Then we will move to the next step to calculate p_{wf} using Eq. (2.33). Comparing with the true p_{wf} which is a given parameter, if they are same then we calculate the flow rate and pressure distribution in the fracture. If it is not, then we increase or decrease the $p_{inner,circle2}$ value to iterate again until the p_{wf} is converged.

2.1.8 Solution for Multi-Fractures System

A schematic of transverse fractures with a horizontal well is illustrated in **Fig.12**. As a simple example, we consider a two-transverse-fracture. For transverse fractures intercepting a horizontal well, the fractures are represented as infinitely conductive or with uniform flux under the assumption that the fractures are dominating the total production to the well. Each fracture can be treated as an individual source and their effects to other fractures are included through the superposed pressure drawdown.

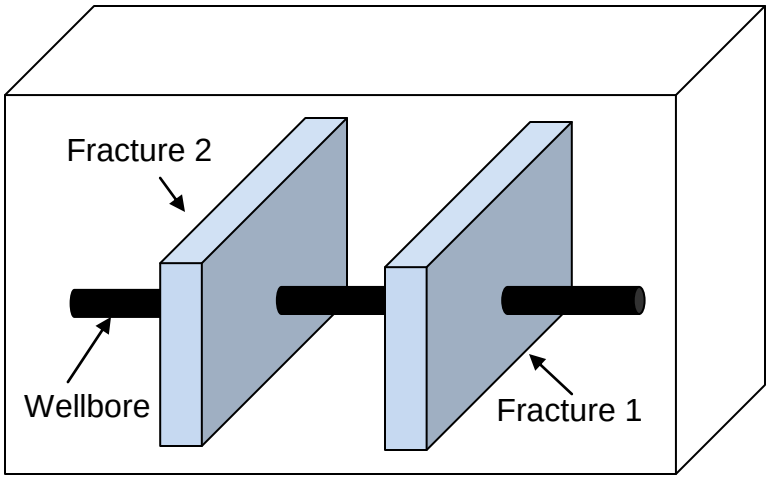

Fig. 12—Transverse fractures along a horizontal well.

Eq. (2.22) can be directly used in this case. In the equation **i** denotes the location that observes the pressure change, and **j** denotes the fracture that causes the pressure change. If considering pressure drop in the wellbore between fractures, then

$$p_{wf,i} - p_{wf,i-1} = \Delta p_{wellbore,i} \tag{2.38}$$

To calculate the well performance, we first place fracture 1 in the system, which causes a flow rate of q_1 at the location of the fracture 1. The flow results in corresponding pressure changes at both locations of the fracture 1 and the fracture 2. Then if assume only fracture 2 exist, the pressure also changes at both locations. Since the total pressure drawdown at each fracture should be the sum of the pressure drops caused by all the fractures in the system, by the superposition principle, we have

$$p_{\text{int}} - p_{1(x,y,z,t)} = F(x,y,z,t) * q_1$$

$$p_{\text{int}} - p_{2(x,y,z,t)} = F(x,y,z,t) * q_2 \tag{2.39}$$

The pressure drop inside the wellbore relates the wellbore flowing pressure $p_{wf,1}$ and $p_{wf,2}$ (Economides, el.at, 1993)

$$p_{wf,1}^2 - p_{wf,2}^2 = \frac{1.007*10^{-4}\gamma_g f_f ZTq_1^2 L}{D^5} \tag{2.40}$$

The pressure drop along the fracture could also be studied. We divided the fracture into N*N segments which are connected to each other by super position. An example of a horizontal well with two transverse fractures is presented here by dividing each fracture into 9 segments, as shown in **Fig. 13**.

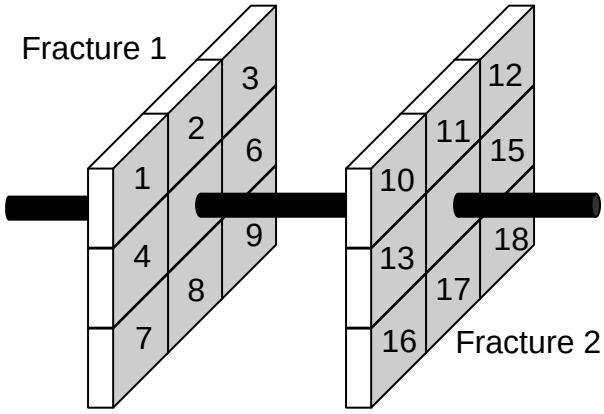

Fig. 13—Transverse fractures with segments.

The well is controlled by a constant wellbore pressure. First the fractures are divided into 9 segments. Starting from the first segment, we calculate the pressure drop at the middle of each fracture segment of the fracture as a result of a constant flow rate, q_1 using Eq. (2.22). This calculation gives 18 F(1, j) terms (one term per segment). Then

we move to the next segment (segment 2) and repeat the same procedure but for this segment we evaluate the pressure drop as a result of constant flow, q_2, flowing into segment 2 which gives another 18 F(2, j). We continue this calculation to the last segment. At this point we will obtain totally 18*18 F(i, j) terms. Then we use the superposition principle in space to connect the wellbore segments. This yields a set of linear equations.

$$q_1F(1,1)+q_2F(1,2)+q_3F(1,3)+...+q_{18}F(1,18)=p_{\text{int}}-p_1$$

$$q_1F(2,1)+q_2F(2,2)+q_3F(2,3)+...+q_{18}F(2,18)=p_{\text{int}}-p_2$$

$$q_1F(3,1)+q_2F(3,2)+q_3F(3,3)+...+q_{18}F(3,18)=p_{\text{int}}-p_3$$

.
.
.

$$q_1F(18,1)+q_2F(18,2)+q_3F(18,3)+...+q_NF(18,18)=p_{\text{int}}-p_{18} \qquad (2.41)$$

The series of linear equation can be written as Eq. (2.41). Then we solve this linear system by defining the inner boundary condition.

The matrix solver used here already encountered the inverses of matrices if it is nonsingular. Gauss-Jordan elimination is used to determine whether a given matrix is invertible and find the inverse. Gauss-Jordan elimination is an algorithm for getting matrices in reduced row echelon form using elementary row operations. It is a variation of Gaussian elimination. Gaussian elimination places zeros below each pivot in the matrix, starting with the top row and working downwards. Matrices containing zeros below each pivot are said to be in row echelon form. Gauss-Jordan elimination goes a

step further by placing zeros above and below each pivot; such matrices are sid to be in reduced row echelon form. Every matrix has a reduced row echelon form, and Gauss-Jordan elimination is guaranteed to find it.

If Gauss-Jordan elimination is applied on a square matrix, it can be used to calculate the matrix's inverse. This can be done by augmenting the square matrix with the identity matrix of the same dimensions and applying the following matrix operation.

$$[AI] \Rightarrow A^{-1}[AI] \Rightarrow [IA^{-1}] \tag{2.42}$$

2.1.9 Non-Darcy Flow

The existence of non-Darcy effects in the flow of fluids through porous media has been studied by petroleum industry for many years; however, characterizing and assessing in magnitude of these effects is still proved difficult.

Henry Darcy developed flow correlation through sand pack configurations in 1856 by flowing water at the local hospital. His results are based on a series of experiments on water flow through a sand packed column at various pressure differentials. From these various experiments he concluded that flow rate varied in proportion to the imposed head and inversely to the height of the sand pack. Darcy's law describes that the linear proportionality which is in Eq. (2.43) involving a constant, k, is related to the potential gradient $\partial p/\partial L$, the fluid viscosity of μ, and the superficial velocity of v.

$$\frac{\partial p}{\partial L} = \frac{\mu \upsilon}{k} \tag{2.43}$$

In 1901, Forchheimer Observed that the deviation from linearity in Darcy's law increased with flow rate. He proposed a second proportionality constant to describe the increasing pressure drop caused by inertial losses. He assumes that Darcy's Law is still valid, but added an additional pressure drop. The familiar Forchheimer equation is shown in Eq. (2.44)

$$\frac{\partial p}{\partial L} = \frac{\mu \upsilon}{k_f} + \beta \rho \upsilon^2 \tag{2.44}$$

When the flow velocity is low, the second term in Eq. (2.44) can be neglected. However, for higher velocities this term becomes more important, especially for low viscosity fluids. If dividing Eqs.(2.43) and (2.44) by $\mu_g \nu$ we obtain

$$\frac{\partial p}{\partial L \mu \nu} = \frac{1}{k_f} \tag{2.45}$$

for Darcy flow and

$$\frac{\partial p}{\partial L \mu \nu} = \frac{1}{k_f} + \frac{\beta \rho \upsilon^2}{\mu \nu} \tag{2.46}$$

for non-Darcy flow. Comparing Eq. (2.45) and (2.46) we see that the effective permeability (determining the actual pressure drop) is

$$k_{f-eff} = \frac{k_f}{\left(1 + \frac{\beta k_f \rho \nu}{\mu}\right)} \tag{2.47}$$

The second term in the denominator of the right-hand side is dimensionless and acts as a Reynolds Number for porous media flow. The Reynolds number in a porous media can be defined as

$$N_{\mathrm{Re}} = \frac{\beta k_f \rho \nu}{\mu} \tag{2.48}$$

where, k_f is in Darcy or cm-g/100sec^2-atm, ρ is in g/cm^3, ν is in cm/s, u_g is in cp or g/100cm-sec and β is in atm-sec^2/gm.

Suggested by Geertsma (1974) , substituting Eq. (2.48) into Eq. (2.47), the final expression of $k_{f\text{-}eff}$ describing the non-Darcy flow effects is

$$k_{f-eff} = \frac{k_f}{(1 + N_{\mathrm{Re}})} \tag{2.49}$$

where velocity ν in Eq.(2.48)

$$\nu = 0.353 \frac{q}{A} \tag{2.50}$$

where, q is in Mscf/day and A is in ft^2.

In hydraulic fracturing operations, the non-Darcy flow effect has been addressed by Cooke (1973). The oil industry attempts to study the impact of non-Darcy effects under different producing situations in the past several years. Non-Darcy effects can significantly decrease well production especially in high flow rate well. Smith, et al (2004), claimed that non-Darcy flow effects decrease 35% in productivity in a hydraulically fractured high rate oil well. They also showed a productivity index reduction of 20% in a high rate (120 MMscf/d) gas well. Cramer (2004) also concluded that “Non-Darcy flow in the fracture exists to some extent in most gas well completions.

It will show up as a rate dependent pseudo-skin, reducing the calculated effective x_f (half-length)" in an extensive analysis of non-ideal cases.

The non-Darcy effect calculation, β is one of the important parameters. β factor is a property of the porous media. The equations have been developed to estimate this factor is based on lab data. Cooke (1973) first developed equation to estimate β factor of proppants. Brady sand was used in the lab experiments. Based on the form of the Forchheimer equation presented in Eq. (2.49), Cooke plotted $\frac{\partial p}{\partial L \mu v}$ vs $\frac{\rho v}{\mu}$ to get the β factor, which is the slope of the curve on the plot. Five sand sizes and various stress levels were considered. The fluids used were brine, gas and oil. Cooke observed no difference of the results among fluids evaluated. All curves followed the simple equation

$$\beta = \frac{a}{k_f^b} \tag{2.51}$$

where, k_f is in Darcy, β is in atm-sec^2/gm, a and b are dimensionless, correlation constants, as shown in **Table 4**.

Penny and Jin (1995) plotted b factor vs. permeability for different type of 20/40 proppants (i.e. northern wide sand, precurred resin coated white sand, intermediate strength ceramic products and bauxite). Final equation developed by them has the same form as Cooke's equation where the coefficients a and b depends on type of sand. These coefficients are shown in **Table 5**. The correlation provides the dry β factor because the authors propose to correct it for multiphase flow (when water or condensate is also flowing).

Table 4— Constants a and b of Cooke's equation.

Sand Size (mesh)	a	b
8/12	3.32	1.24
10/20	2.63	1.34
20/40	2.65	1.54
40/60	1.10	1.6

Table 5—Constants a and b of Peeny and Jin equation for 20/40 mesh.

Type of proppant	a	b
Jordan Sand	0.75	1.45
Precurred Resin-Coated Sand	1	1.35
Light Weight Ceramic	0.7	1.25
Bauxite	0.1	0.98

As previously discussed, non-Darcy flow in a gas reservoir causes a reduction of the productivity index. The effect on pressure drop and production distribution inside fracture is estimated following the flow chart as shown in **Fig. 14**. Using the slab source method, the flow rate is first calculated with the original proppant. Then the effective proppant permeability is compared with the proppant permeability at the flow rate to check whether they are the same. If it is not, the effective proppant permeability is used to get the new gas production by the slab source method. The iteration stops until the new effective proppant permeability is the same as the previous one. The final proppant

permeability is then used to calculate the pressure and production distribution along the fracture.

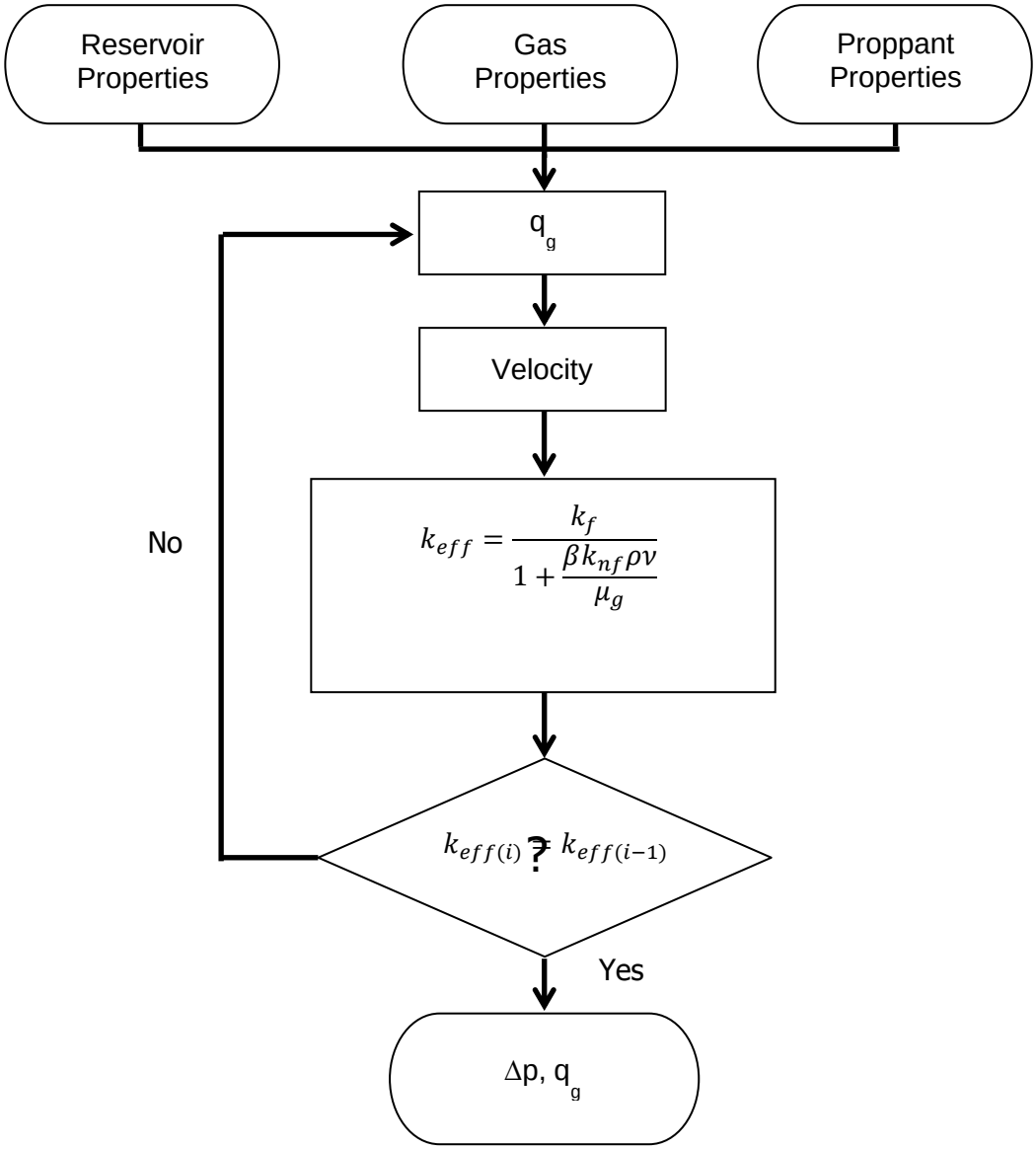

Fig. 14—Flow chart for Non-Darcy flow.

2.1.10 Preliminary Solution for Complex Fracture System

The multiple hydraulic fractures combined with natural fractures create very complex fracture networks. In this study, a simplified hydraulic fracture/natural fracture system is used to illustrate the approach of using the Slab source model to estimate flow rate in such a system.

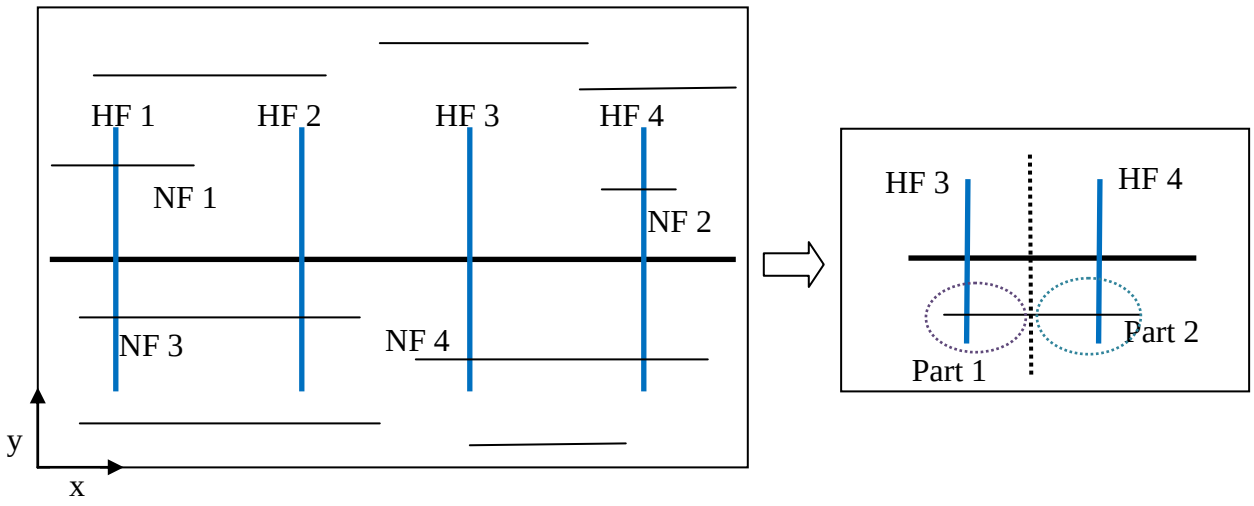

Fig. 15—Schematic of complex fracture system.

Fig. 15 shows the physical model used in the approach. If assuming that the natural fractures that connected to the hydraulically created fractures are all orthogonal to the hydraulic fractures, as shown in **Fig. 15**, then it is assumed that the hydraulic fractures that connect with the wellbore are the main fractures and the natural fractures are branch fractures which only connect with the main fractures, but not the wellbore. The fluid inside the branch fractures directly flows into the main fractures. For the main fractures,

the fluid is from both the reservoir and the connected branch fractures, and it flows to the wellbore. We considered each hydraulic fracture and natural fracture is an individual source, and the sources will be affected by each other. Superposition method is applied in this situation. By inputting properties for the natural fractures and hydraulic fractures, production can be calculated.

The natural fractures are local sources providing flow rate at the locations where they intercept with hydraulic fractures. If a natural fracture intercept move than one hydraulic fracture, such as NF3 and NF4 in **Fig. 15**, the natural fracture will be treated as shown on the right side of **Fig. 15**. The natural fracture is divided into 2 parts, and each part would be treated as a single natural fracture. Then the total flow rate from this natural fracture is the total of the two parts. For example, the flow rate of NF4 is divided by 2 part and we treated it as NF5 and NF6.

The complex system is controlled by a constant wellbore pressure. With the system shown in **Fig. 14**, we have 4 hydraulic fractures, HF1, HF2, HF3, and Hf4; and 4 natural fractures NF1, NF, 2, NF3, and NF4. However, NF3 and NF4 are connected with two Hydraulic fractures, and then the total fracture number should be 10.

We acquire a set of linear equations as shown in Eq.(2.52). Then we solve this linear system by defining the inner boundary condition

$$q_1 F(1,1) + q_2 F(1,2) + q_3 F(1,3) + \ldots + q_{11} F(1,10) = p_{\text{int}} - p_1$$

$$q_1 F(2,1) + q_2 F(2,2) + q_3 F(2,3) + \ldots + q_{11} F(2,10) = p_{\text{int}} - p_2$$

$$q_1 F(3,1) + q_2 F(3,2) + q_3 F(3,3) + \ldots + q_{11} F(3,10) = p_{\text{int}} - p_3$$

.

.

$$q_1 F(10,1) + q_2 F(10,2) + q_3 F(10,3) + \ldots + q_{11} F(10,10) = p_{\text{int}} - p_{10} \qquad (2.52)$$

CHAPTER III

VALIDATION

The solution presented in Chapter 2 is validated by the solutions of different methods. For horizontal wells, we compared the solution with an analytical solution presented by Babu and Odeh (1988), and for fracture cases, we validated the slab source model with the volumetric source model (Valko and Amini, 2007) and commercial software, Ecrin-Kappa (Version 4.12). We validated the complex fracture system case with the ECLIPSE (Schlumberger).

3.1 Uniform Flux Horizontal Well

Babu and Odeh (1988) presented a method to obtain the performance of a horizontal well. They developed a line source solution to represent a horizontal well. The model is under pseudo-steady state condition. The input data is given in **Table 6**. Comparing the slab source model with Babu and Odeh's model, **Fig. 16** shows the results of the two solutions for the example of uniform flux horizontal well. The result of the slab source model agrees with the Babu and Odeh's model. Since Babu and Odeh's model assumed pseudo-steady state boundary, the reservoir pressure is an average pressure over the reservoir volume, but the slab model is a transient model and pressure declines from the initial reservoir pressure. We used the material balance to approximate the average

reservoir pressure decline when using Babu and Odeh's model, which causes the difference between the results of the two models.

Table 6—Input data for horizontal well validation.

Parameter	Value	Unit
Reservoir length (assumed), b	4000	ft
Reservoir width (assumed), a	2000	ft
Reservoir thickness, h	200	ft
Horizontal wellbore length, L	3000	ft
Porosity, ϕ	9.0%	
Reservoir initial pressure, p_i	2335	psi
Reservoir temperature, T	146	°F
Bottomhole pressure, p_{wf}	1886	psi
Gas specific gravity, γ_g	0.836	
Water specific gravity, γ_w	1.005	
Gas component $\begin{cases} H_2S \\ CO_2 \\ N_2 \end{cases}$	0%	
	1%	
	1.4%	
Reveal Data		
Horizontal permeability, k_h	0.25	md
Vertical permeability, k_v	0.1	md
Gas viscosity, μ_g	0.0156	cp

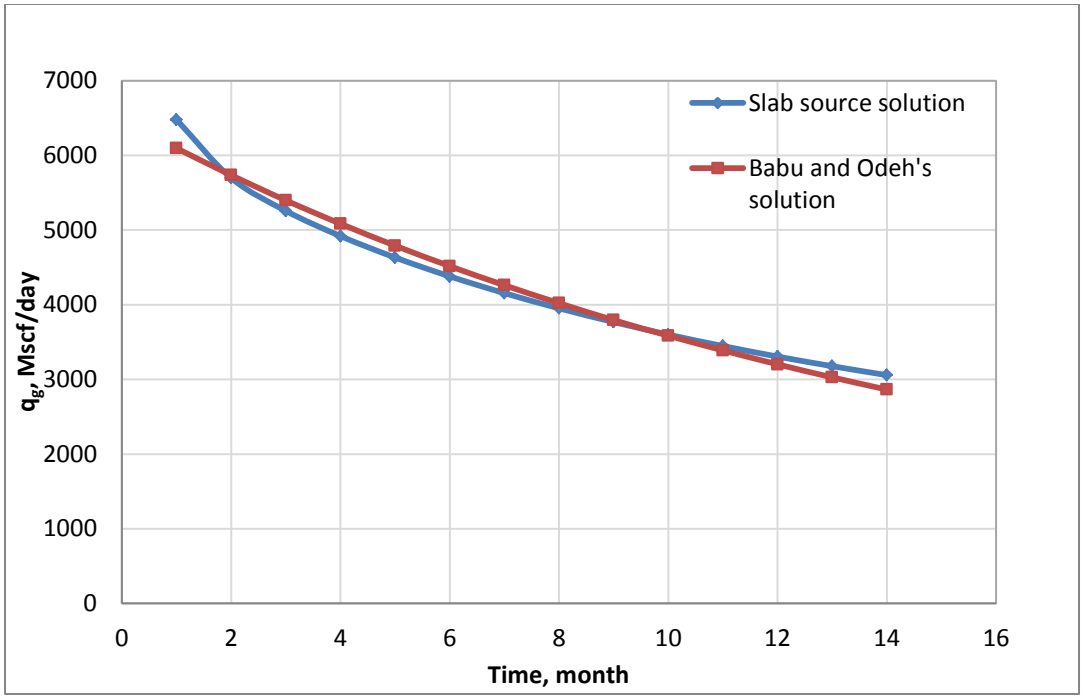

Fig. 16—Comparison of the slab source model with Babu and Odeh's model.

Ouyang (1997) presented a semi-analytical solution to study to horizontal well performance under pseudo-steady state condition by an integrated point source along a well trajectory. The slab source model has been compared with Ouyang's model. The input data is shown in **Table 7**. The results (**Fig. 17**) show that the two methods get the similar results for pseudo-steady state condition. At the beginning of 300 days, the flow rate drops fast and then it is almost flat.

Table 7—Input data for horizontal well validation (2).

Parameter	Value	Unit
Reservoir length (assumed), b	4000	ft
Reservoir width (assumed), a	1000	ft
Reservoir thickness, h	200	ft
Horizontal wellbore length, L	3000	ft
Porosity, ϕ	0.2	
Reservoir initial pressure, p_i	3500	psi
Bottomhole pressure, p_{wf}	2000	psi
Formation volume, B	1.1	bbl/stb
Oil viscosity	1.6	cp
Horizontal permeability, k_h	10	md
Vertical permeability, k_v	10	md
Total compressibility, c_t	$1.25*10^{-5}$	psi^{-1}

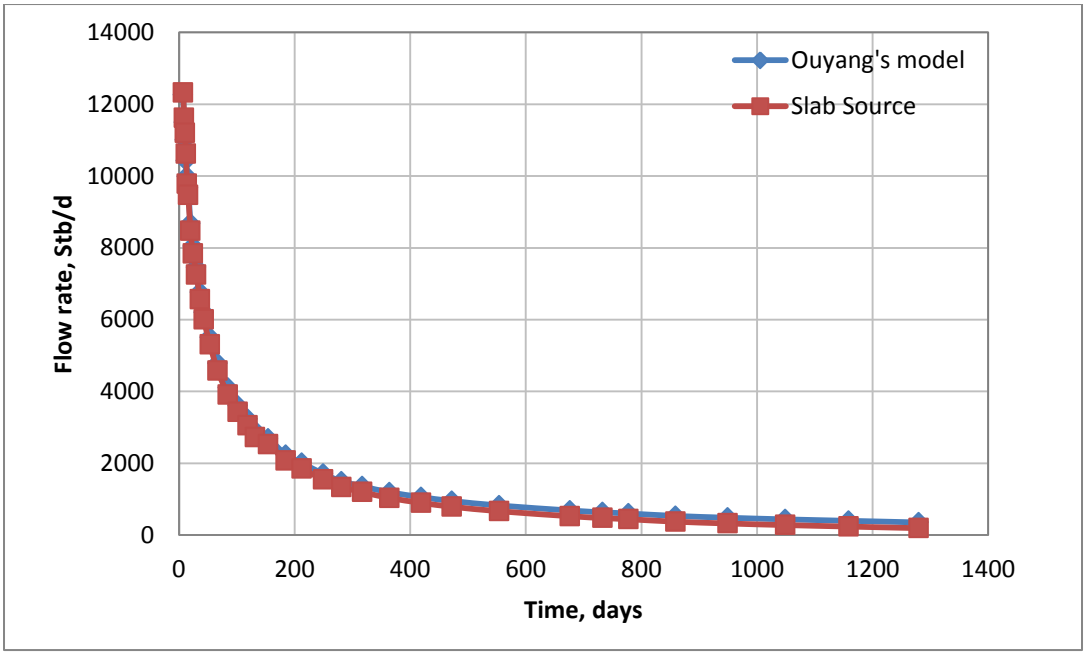

Fig. 17—Comparison of the slab source model with Ouyang's model.

3.2 Fully Penetrating Transverse Fracture Intercepting a Horizontal Well

The input data used in validating the fracture model is shown in **Table 8**. The result of a fully-penetrating transverse fracture with uniform flux is compared with the solution by the distributed volumetric source model (Valko and Amini, 2007) and the commercial software Ecrin-Kappa. In this case, as demonstrated in **Fig. 18**, the three methods showed a good agreement. It should be noticed that the slab source model neglected the pressure drop caused by the Non-Darcy flow inside fracture. For the purpose of comparing with the distributed volumetric source model because this pressure drop is not included in the distributed volumetric methods. When flow rate is high, this assumption is not valid (Miskimins. et. al, 2005) and could result in some errors in rate estimation.

From the comparisons with other models at the appropriate conditions, we validated of the slab model for horizontal wells with an excellent agreement for uniform flux and infinite conductivity solution. For the case of fractured wells, the results are in very good agreement (within 1% difference).

Table 8—Input data for single transverse fracture validation.

Parameter	Value	Unit
Reservoir length (assumed), b	4000	ft
Reservoir width (assumed), a	2000	ft
Reservoir thickness, h	200	ft
Porosity, ϕ	0.09	ft
Reservoir initial pressure, p_i	2335	psi
Reservoir temperature, T	146	°F
Bottomhole pressure, p_{wf}	1885	psi
Gas specific gravity, γ_g	0.836	
Horizontal permeability, k_h	0.5	md
Vertical permeability, k_v	0.25	md
Gas viscosity, μ_g	0.0156	cp
Fracture length, L_f	1000	ft
Fracture height, h_f	100	ft
Fracture width, w_f	0.033	ft

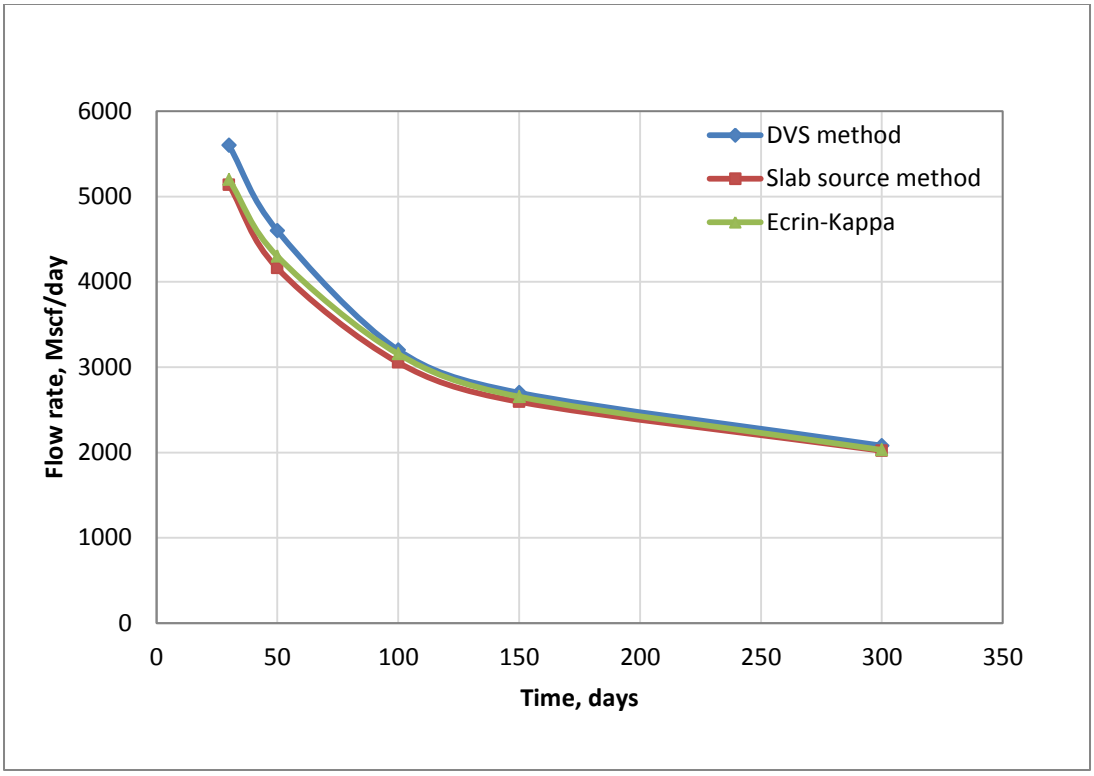

Fig. 18— Comparison of the slab source model with DVS and simulation by Ecrin.

3.3 Segment-source for Single Fracture

In the slab model, each fracture is divided into multiple segments in order to account for the pressure drop inside the fractures. To validate this approach, a transverse fracture is divided into 4 or 9 segments in this study. The wellbore is placed in the middle of the fracture. Superposition method has been applied to the problem. If we assume that the pressure for each segment is equal to the wellbore pressure, then the production from each segment will be equal, so does the total flow rate from the cases with different

segment number. In addition, the total flow rate should be equal to the rate from non-segment fracture model if neglecting the pressure drop inside the fracture. We use this to validate the superposition operation. The input data is given in **Table 8**. The example shown here is to validate the superposition method which is used in our model. By checking whether the total flow rate is the same no matter of how many segments the fracture has. From the results (**Fig. 19**), the production rates for 1, 4 and 9 sources are the same, which confirms the superposition method we used in the study. More segment number can be used to count for conversion in the fracture. The effect of heterogeneity in the reservoirs can also be studied by this method by assigning different permeability to different segments.

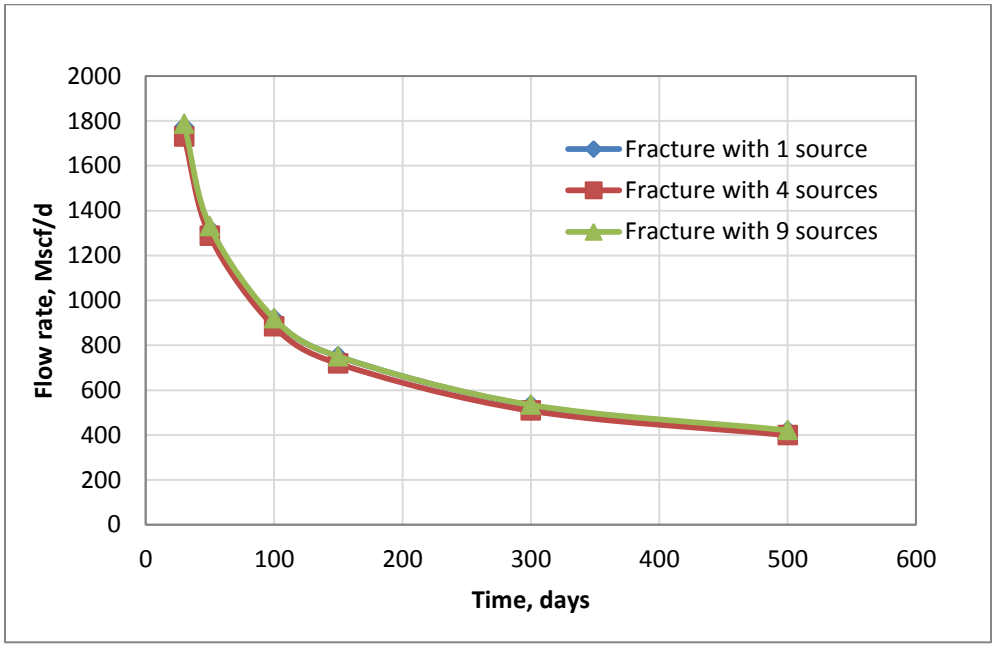

Fig. 19—Comparison of superposition procedure.

3.4 Complex Fracture System vs ECLIPSE

For complex fracture system, we use a simple example to compare our results with a commercial simulation result (ECLIPSE 100, Schlumberger). The input parameters are list in **Table 9**. The schematic of complex fracture system is show in **Fig. 20**.

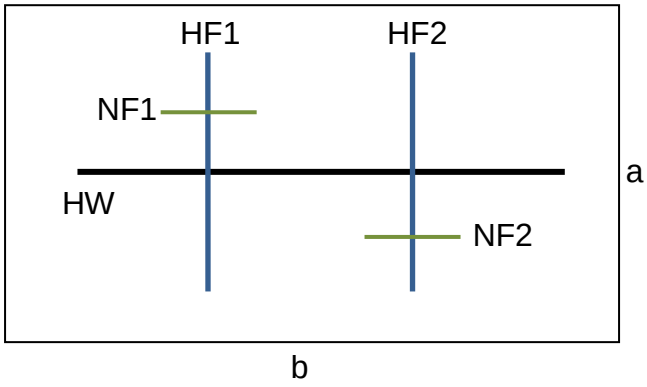

Fig. 20—Complex fracture system schematic.

Fig. 21 and **22** present comparison of the two methods. They show a good match. **Fig. 21** shows the flow rate drop quickly at the beginning of the time. For slab source model (**Fig. 22**), shows the similar results and reaches the pseudo-steady state flow at the time of 300 days.

Table 9— Input data for complex fracture validation.

Parameter	Value	Unit
Reservoir length (assumed), b	2000	ft
Reservoir width (assumed), a	1000	ft
Reservoir thickness, h	100	ft
Porosity, ϕ	0.09	ft
Reservoir initial pressure, p_i	2200	psi
Reservoir temperature, T	146	°F
Bottomhole pressure, p_{wf}	1800	psi
Gas specific gravity, γ_g	0.836	
Horizontal permeability, k_h	0.01	md
Vertical permeability, k_v	0.001	md
Gas viscosity, μ_g	0.0156	cp
Horizontal well length, L	1500	ft
Hydraulic Fractures		
Fracture length, x_f	250	ft
Fracture height, h_f	100	ft
Fracture width, w_f	0.033	ft
Natural Fractures		
Fracture length, x_f	125	ft
Fracture height, h_f	50	ft
Fracture width, w_f	0.008	ft

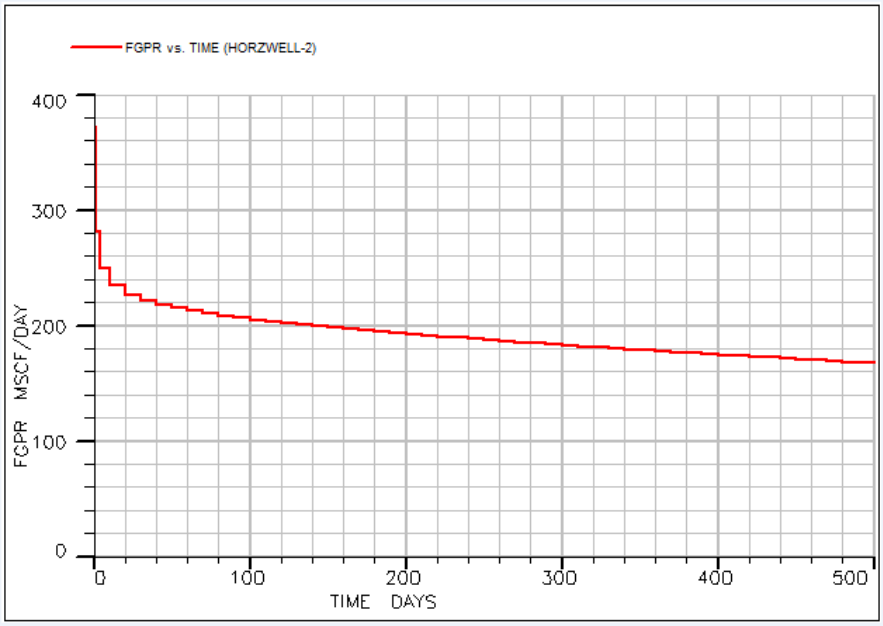

Fig. 21—ECLIPSE simulation results.

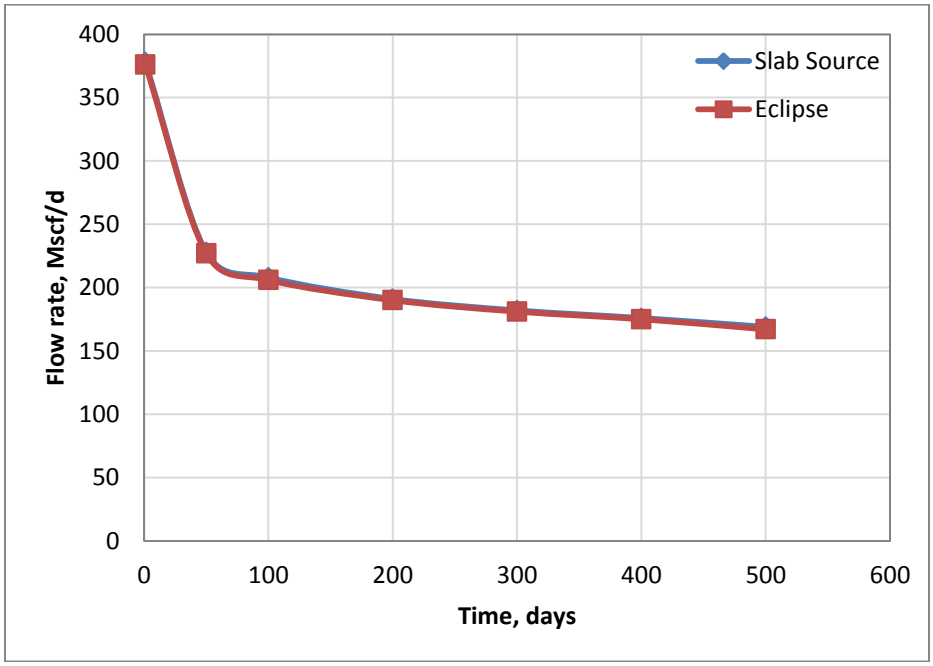

Fig. 22—Slab source model results.

CHAPTER IV

RESULTS AND DISCUSSION

In this chapter, the Slab source method is applied to cases of complex well or fractured horizontal well schematic to show how to optimize the production of such wells by using the developed method.

Examples of horizontal well with different wellbore length, a horizontal well with single or multiple transverse fractures intercepts horizontal well are presented first. Then three field examples are used to show the procedure of the model application with one example for low permeability unconventional reservoir, and the other moderate permeability conventional reservoir.

4.1 Synthetic Model

In this section, synthetic examples are used to illustrate how to use the Slab model to optimize well design for horizontal wells and horizontal wells with fractures. The input data used in this section is shown in **Table 10.**

Table 10—Input data for synthetic examples.

Reservoir type	Tight gas	
Formation type	Sandstone	
Parameter	Value	Unit
Reservoir length (assumed), b	4000	ft
Reservoir width (assumed), a	2000	ft
Reservoir thickness, h	200	ft
Horizontal wellbore length, l	1000, 2000, 3000, 3500	ft
Porosity, ϕ	9.0%	
Reservoir initial pressure, p_i	2500	psi
Reservoir temperature, T	146	°F
Bottomhole pressure, p_{wf}	1800	psi
Gas specific gravity, γ_g	0.836	
Reveal Data		
Horizontal permeability, k_h	0.1, 0.01, 0.001	md
Vertical permeability, k_v	0.01, 0.001, 0.0001	md
Gas viscosity, μ_g	0.0156	cp

4.1.1 Horizontal Well

To product tight gas reservoir, horizontal wells are more efficient compared with vertical wells. The length of the horizontal laterals relative to the reservoir drainage dimension will is a key parameter for well production. In general, for tight formation since mobility dominates the production, the longer the wellbore length, the higher the production rate. Comparing to the drawdown of the reservoir, the pressure drop along the wellbore is usually not significant, therefore the pressure drop along the wellbore is neglected in

these examples. The well was placed in the middle of the reservoir. **Fig. 23** is the schematic for this study. This resembles an open-hole completion.

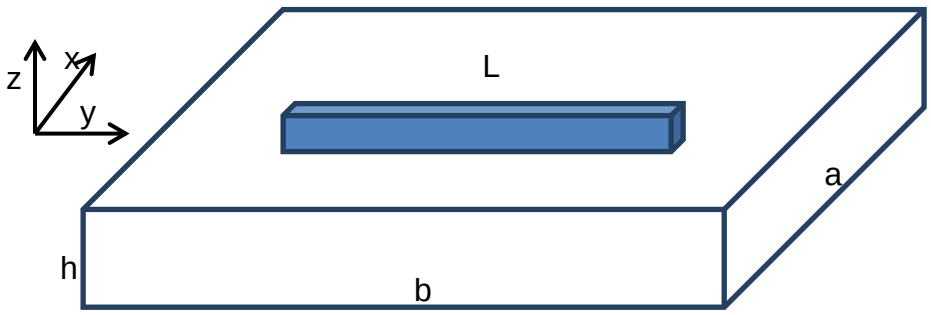

Fig. 23—Set up for horizontal well.

Fig. 24 and **25** show the production performance for the horizontal well under transient flow condition for relatively low permeability (0.01-md, in **Fig. 24**), and moderate permeability (0.1-md, **Fig. 25**). At the same drawdown, with low permeability, longer wellbore keeps significant advantage through the production period of 500 days (**Fig. 24**), but for higher permeability (0.1-md), the benefit of longer wellbore diminishes and rate declines much faster for longer wellbore compared with short wellbore (**Fig. 25**). It is necessary to point out that when permeability is higher than 0.1-md, the initial rate is significant and pressure drop in the wellbore should be considered in this case.

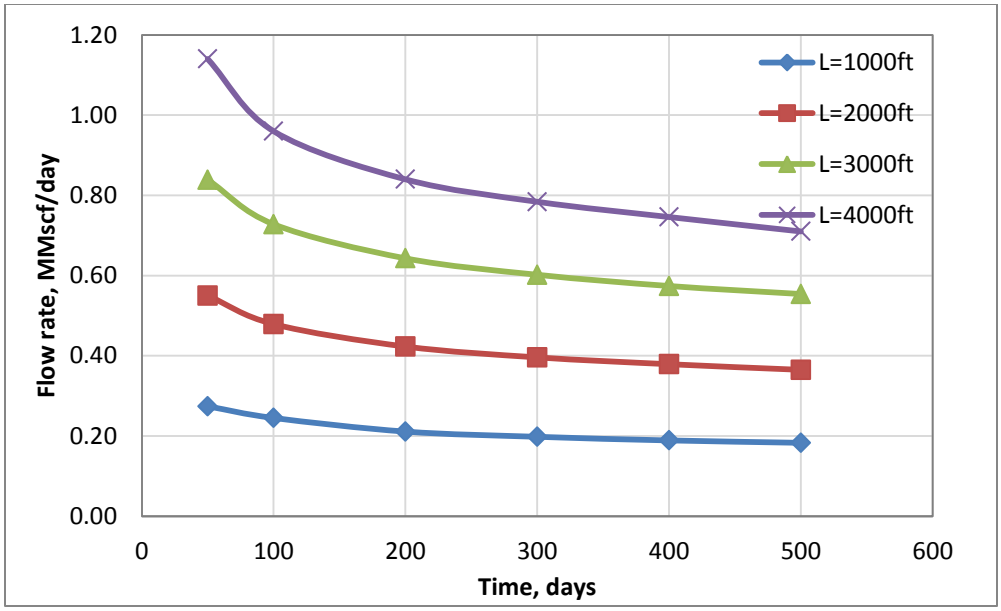

Fig. 24— Effect of wellbore length on production rate for k_h=0.01md, k_v=0.005md.

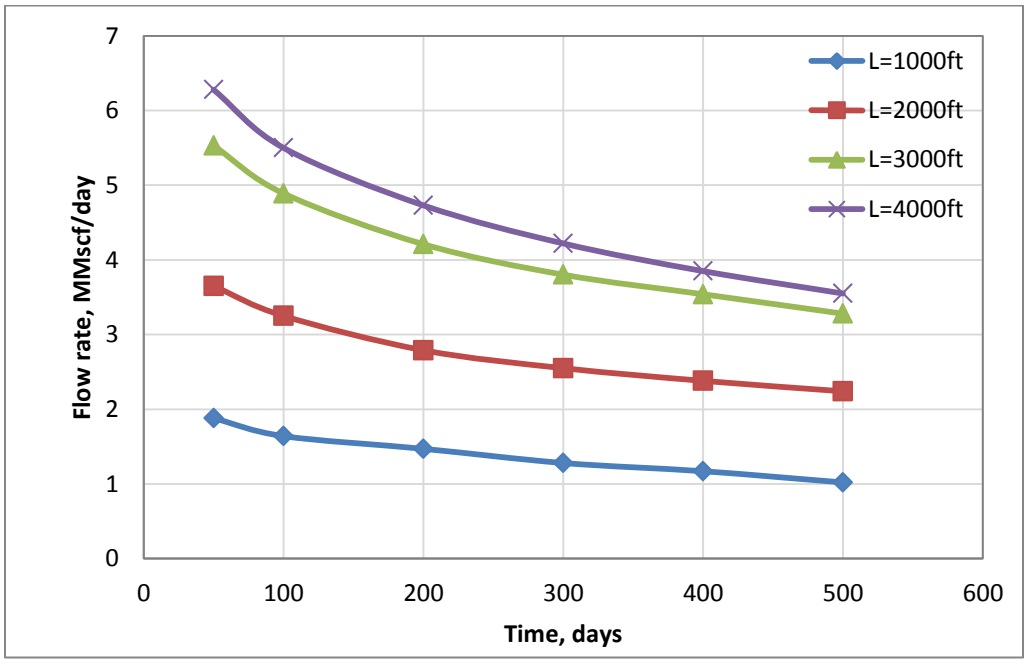

Fig. 25— Effect of wellbore length on production rate for k_h=0.1md, k_v=0.01md.

The advantage of a longer well length reaches a plateau when the wellbore length is close to the reservoir dimension. Since longer length will cost more in drilling and completion, there should be an optimal length which is not only directly related to the reservoir dimension but also affected by the reservoir properties, such as permeability. As shown in **Fig. 26**, the longer the wellbore is, the better the production is. For relatively low permeability reservoir, the performance will be good when a really long horizontal wellbore placed in reservoir. **Fig. 27** and **28** show that after 3000-ft length, the production increase reaches a plateau. Beyond this point, increasing wellbore length will no increase the production rate enough to justify the addiction costs of creating a longer wellbore. For different reservoir conditions, the optimal length varies, and the optimal length should be identified for individual cases. This can be clearly demonstrated that when permeability is relatively low the horizontal well would be benefit compared to moderate permeability reservoir. In the same reservoir dimension, the longer the wellbore length in low permeability gives more production increase ration compared to the one in high permeability.

Realizing that even the flow rate of horizontal wells in low permeability formations may not be high enough to cause a significant pressure drop in the wellbore, it does not limit the case that frictional pressure will affect the well performance. When wellbore length increases it will increase the frictional pressure in the wellbore in two counts: longer horizontal wells can also limit the well performance, the pressure drop in the wellbore in such situation should be considered when designing the wellbore length.

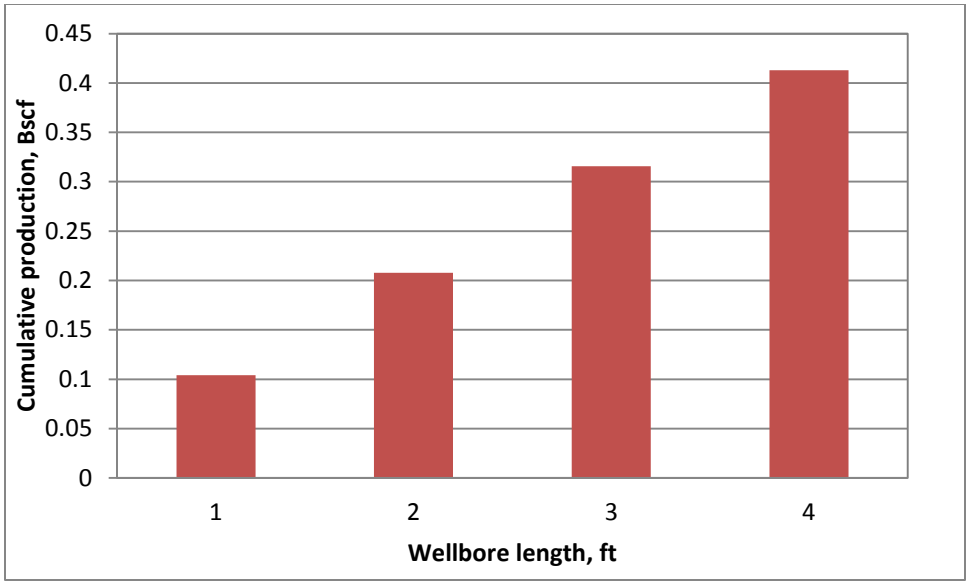

Fig. 26—Effects of wellbore length on cumulative production (k_h=0.01md).

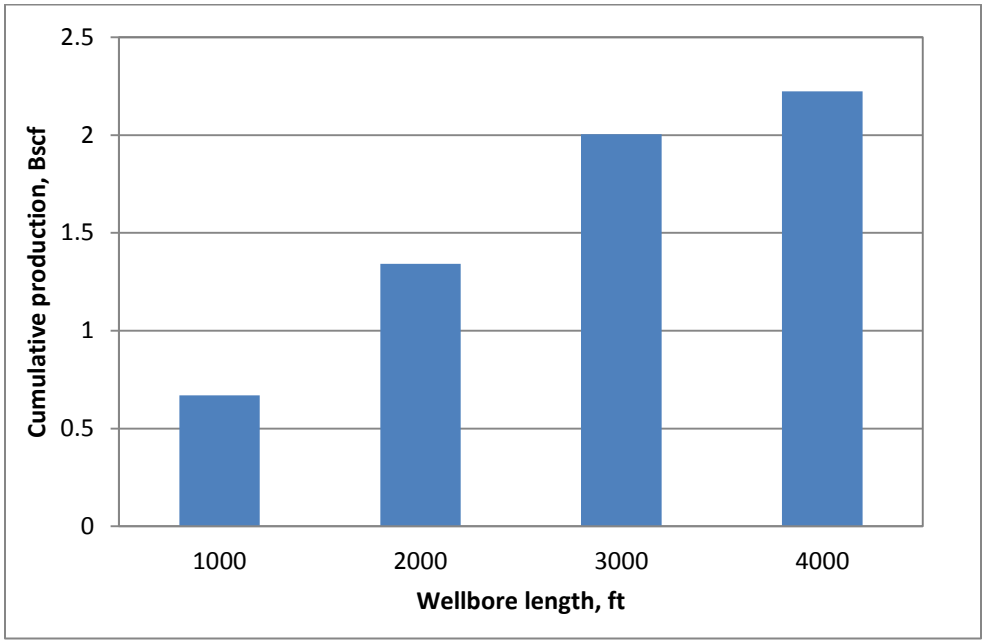

Fig. 27—Effects of wellbore length on cumulative production (k_h=0.1md).

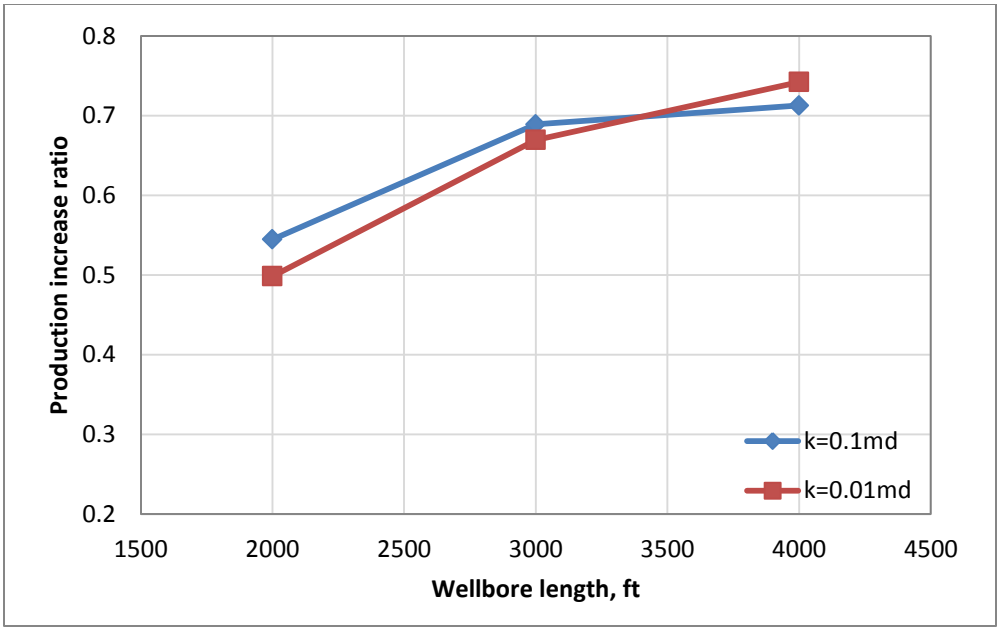

Fig. 28—Percentage increases in cumulative production due to wellbore length increase.

4.1.2 Multiple Fractures with Infinite Conductivity

Superposition method is applied to study the cases of multiple transverse fractures along a horizontal well. We compare the production rate for horizontal well with five, ten, fifteen, and twenty fractures. All the fractures have the same dimensions which are 500-ft (half length)*0.25-in (width)*50-ft (height), and each fracture is treated as one source.

Fig. 29 to **31** show the results of well performances for three different reservoir permeabilities. For a high-perm gas reservoir, fracture number is a sensitive parameter to make hydraulic fracturing attractive. When the number of fractures is too high, benefit of adding more fractures diminishes. For low-perm gas formations, wells with more fractures are more likely to perform better than wells with fewer fractures. The more

fractures that can be placed along the wellbore, the higher production rate will be. As studied before (Zhu et al., 2007; Bagherian et al., 2010), there may be a maximum number of fractures, and above that number, more fractures will not bring more benefit to the well production. The optimal fracture spacing also depends on the stress field change while fracturing each stage (Roussel and Sharma, 2010; Suri and Sharma, 2009), and completion limitations (how many fractures can actually be placed along a wellbore). All these should be considered when design a multi-stage fracture treatment in additional to maximum production rate.

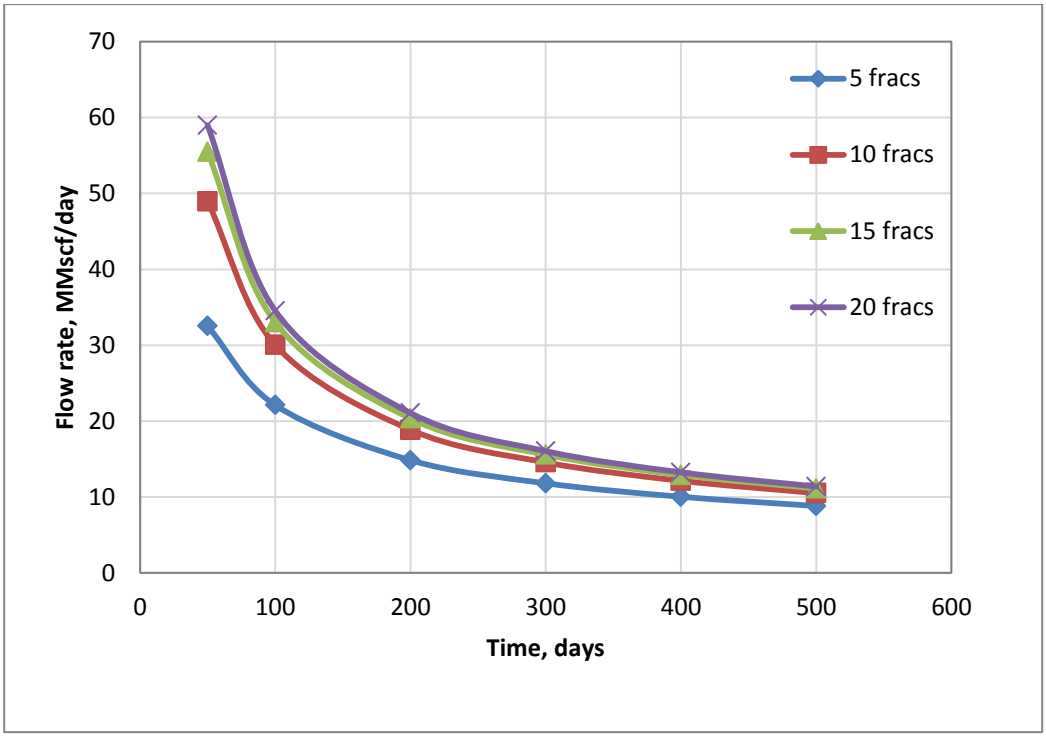

Fig. 29—Cases comparison for k_h=0.1md and k_v=0.01md.

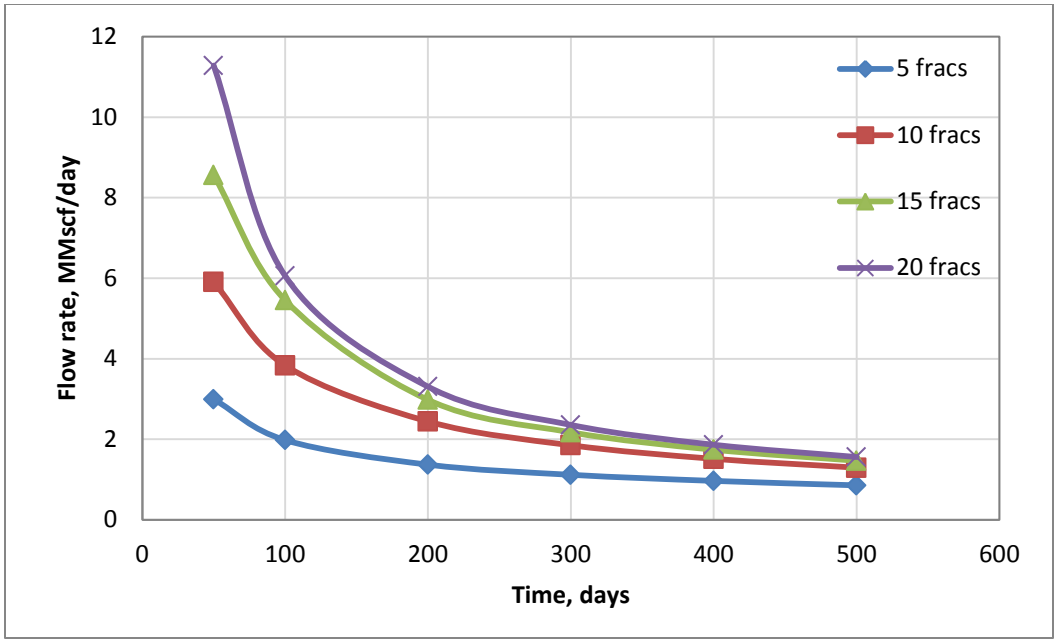

Fig. 30— Cases comparison for k_h=0.01md and k_v=0.001md.

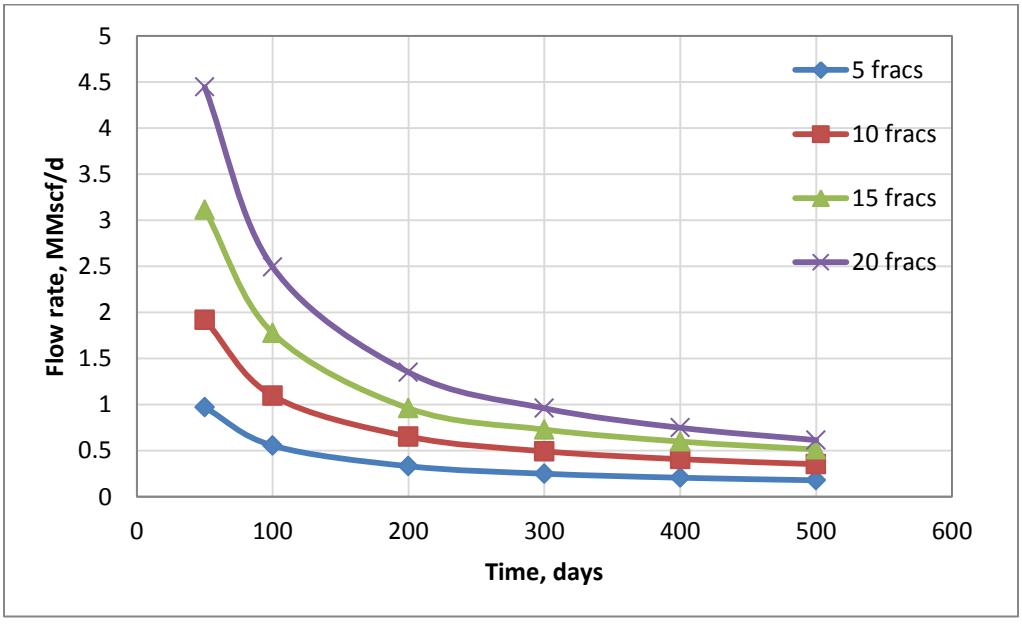

Fig. 31— Cases comparison for k_h=0.001md and k_v=0.0001md.

Noticed that the results show that a horizontal well with 20 fractures produces about five times more than the production rate of a horizontal well with 5 fractures at early time of production when reservoir permeability is 0.001md. The reason is that for more fractures, the sources are more evenly distributed in the reservoir, and traveling distance for the reservoir fluid to research the sources (one of the fractures) becomes smaller, implying that flow efficiency is improved with more fractures placed along the wellbore. For reservoir permeability is 0.1-md, the well with 15 and 20 fractures shows almost the same production rate in **Fig. 29**, which means in such a reservoir, more fracture number will not give us more benefit on production. It suggests that ten fractures should be enough for this reservoir. When reservoir permeability is drop to 0.01-md (**Fig. 30**), the horizontal well with 15 fractures still produces significantly more than 10 fractures. But when placed 20 fractures, the production rate does not increase much compared with 15 fracture case; which means that the fracture number around 15 is optimal for this reservoir. For reservoir permeability of 0.001-md (**Fig. 31**), the horizontal well with 20 fractures still gives us a high production rate. We could draw the conclusion that in extremely low (0.001-md) permeability reservoir, the more hydraulic fractures, the more it will benefit to the production.

Fig. 32 shows that after 15 fractures, the production increase (rate at any fracture number compared with the rate at 5 fractures) approaches a constant for k=0.1-md. Beyond this point, increasing fracture number will not increase the production rate enough to justify the addiction costs of creating a longer wellbore. For different reservoir conditions, the optimal fracture number should be identified for individual cases. We

also notice that the production increase for k=0.001-md is four times higher compared to k=0.1-md condition, which is could also draw the conclusion that hydraulic fractures is an effective way to develop the reservoir with low permeability.

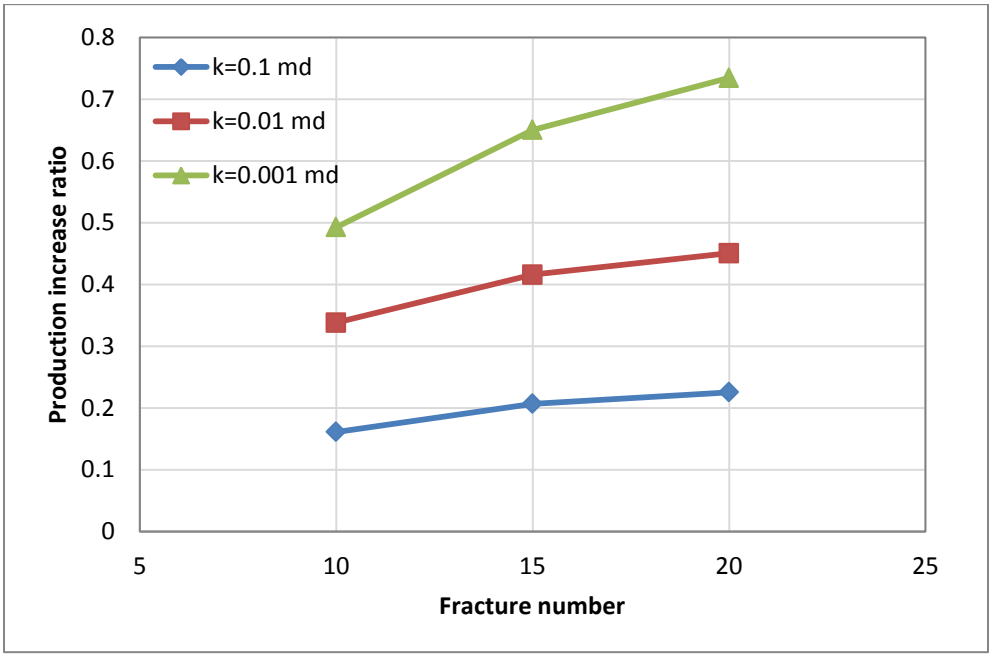

Fig. 32—Production increase ratio as a function of number of fractures.

4.1.3 Fracture with Finite Conductivity

To study pressure drop inside the fracture, we divided the fracture into several segment. The fracture pressure profile under finite conductivity inner boundary condition is shown in **Fig. 33**. It presents that the pressure decreases from the outside boundary to the center of the fracture. The production distribution is shown in **Fig. 34**. In this case, we have

five fractures along the horizontal well and each fracture has 9 segments. Because of the pressure drawdown, the production rate is lower than infinite conductivity condition.

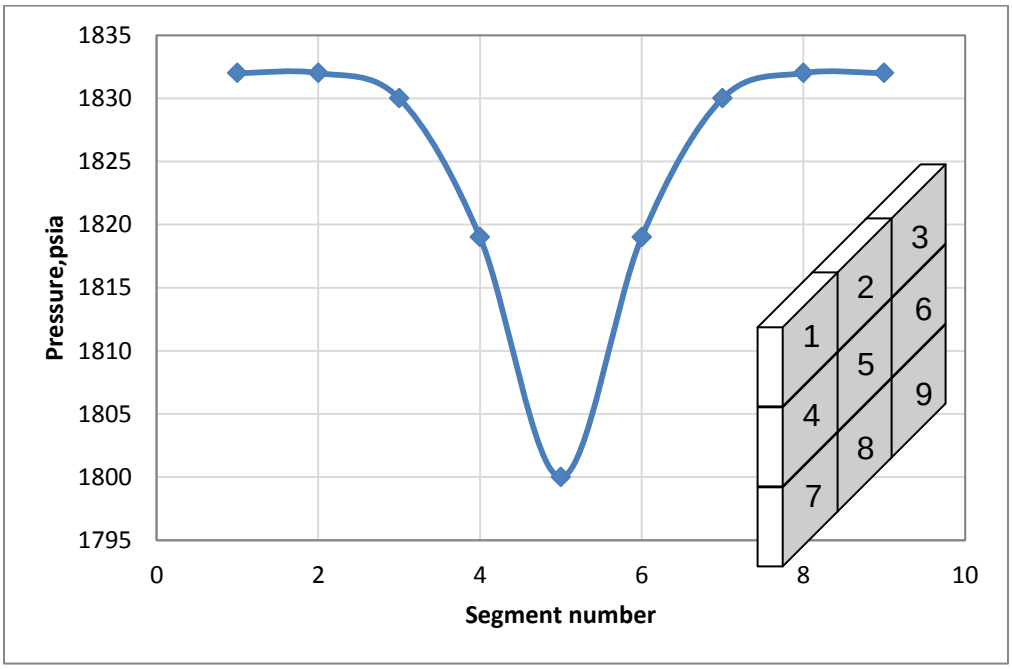

Fig. 33—Fracture pressure profile for k_h=0.1md, k_v=0.01md, and k_f=50000md.

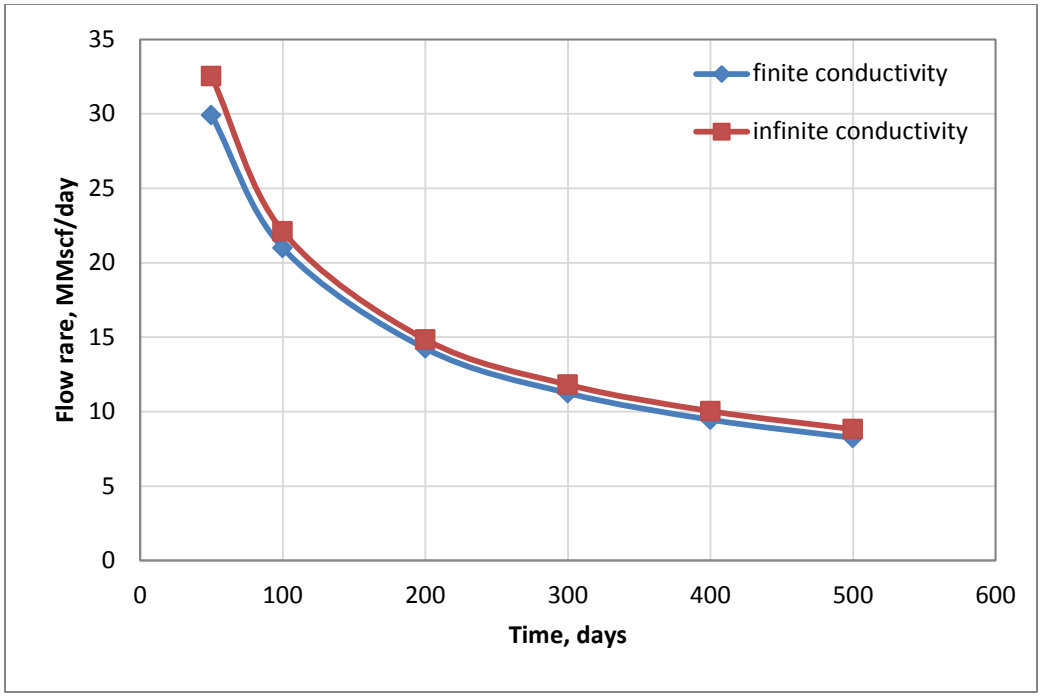

Fig. 34—Infinite conductivity vs. finite conductivity for k_h=0.1md, k_v=0.01md, and k_f=50000md.

Fig. 35 shows the production distribution for each fracture along the horizontal wellbore for 50 days. The profile shows that the flow rate for the first and the last fracture at the both ends of horizontal well are the highest followed by fracture 2 and 4, and the least flow rate is from fracture 3. Since the first and the last fracture have more drainage area compared to the fractures in the middle, the production rate is the highest as show in **Fig. 36**. This additional drainage also contributes to fracture 2 and 4. The fracture 2 and 4 compared with fracture 3 have higher flow rate.

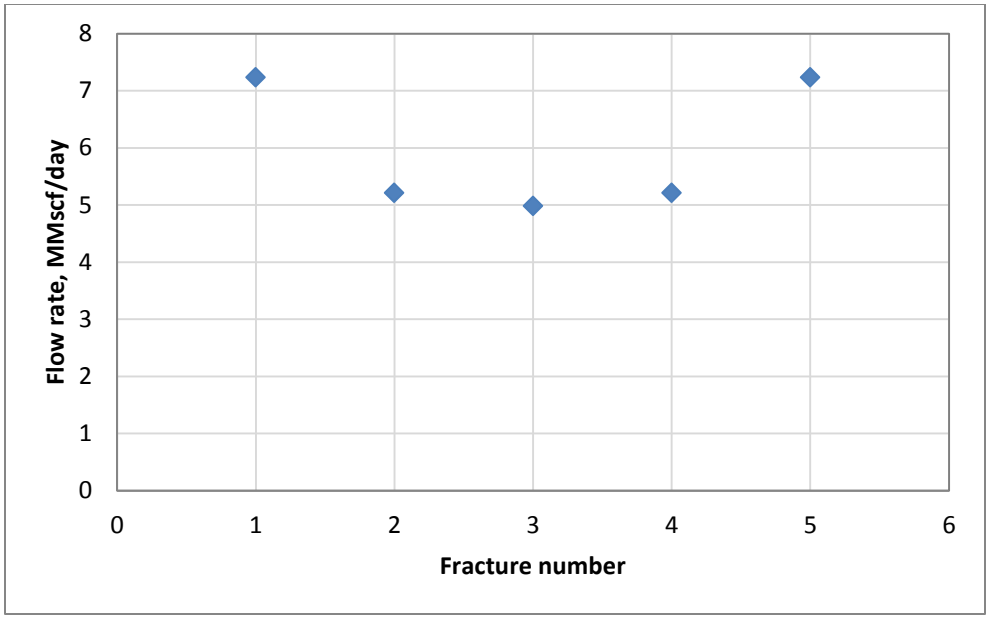

Fig. 35—Flow rate profile for each fracture.

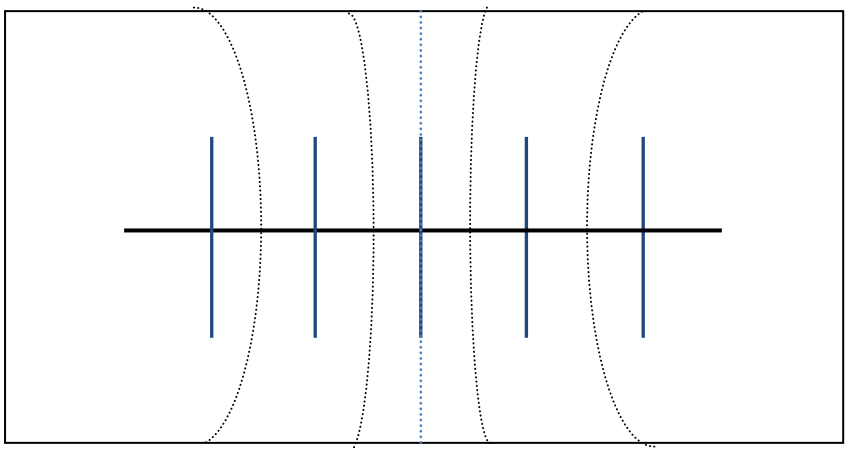

Fig. 36—Flow region for each fracture.

4.1.4 Complex Fracture System

The slab source method could also be used for complex fracture systems. The complex fracture system is defined as multiple hydraulic fractures placed along a horizontal well in a natural fracture formation. The hydraulic fractures that connect with the wellbore are the mean fractures and the natural fractures are branch fractures which only connect with the main fractures. The fluid inside of the branch fractures directly flows into the main fractures. For the main fractures, the fluid of the main fracture is from both the reservoir and the branch fractures and flows to the wellbore. We considered each hydraulic fracture and natural fracture is a separate source, and the sources will be affected by the other sources in the system. Superposition method is applied to capture the internal affection among the sources.

Fig. 37 shows a randomly generate natural fracture network with 20 hydraulic fractures. The natural fracture length is from 100 to 500-ft and the width is 0.08 to 0.1-in. For 20 natural fractures, only seven of them are connected with the hydraulic fractures. One of the natural fractures connects two of the hydraulic fractures. As mentioned before, we divided the natural fracture into two parts and each of them is connect with the hydraulic fractures near it. The input data for this case is shown in **Table 11**.

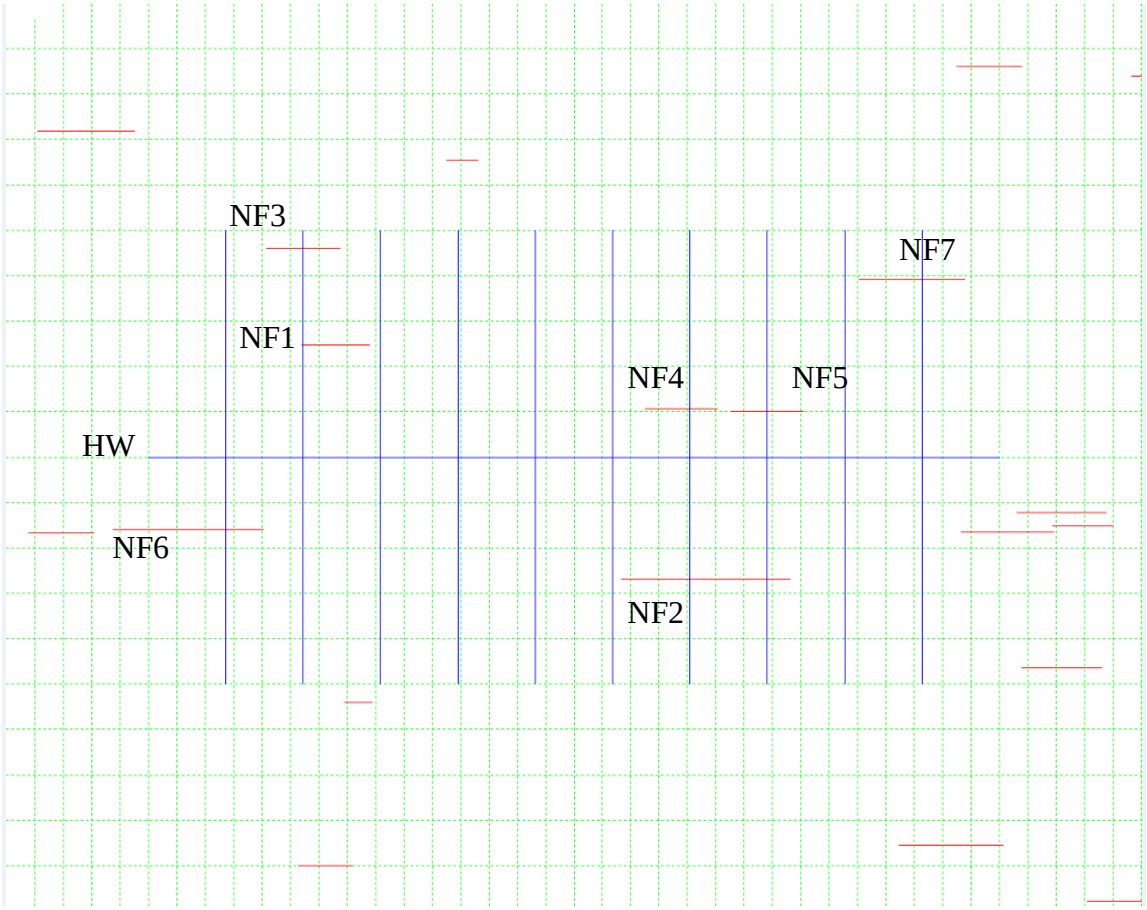

Fig. 37— Randomly generated complex fracture system.

.

The result is shown below in **Fig. 38.** The results show that both the hydraulic fractures and natural fractures would produce. At early time, the hydraulic fractures produce much more than natural fractures, but after 300 days, the flow rate from hydraulic fractures is 4.5 times more than natural fractures.

Table 11—Input data for complex fracture system.

Parameter	Value	Unit
Reservoir length (assumed), b	4000	ft
Reservoir width (assumed), a	2000	ft
Reservoir thickness, h	200	ft
Porosity, ϕ	0.09	ft
Reservoir initial pressure, p_i	2200	psi
Reservoir temperature, T	146	°F
Bottomhole pressure, p_{wf}	1800	psi
Gas specific gravity, γ_g	0.836	
Horizontal permeability, k_h	0.1	md
Vertical permeability, k_v	0.01	md
Gas viscosity, μ_g	0.0156	cp
Horizontal well length, L	3000	ft
Hydraulic Fractures		
Fracture length, x_f	500	ft
Fracture height, h_f	100	ft
Fracture width, w_f	0.033	ft

Natural Fracture No.	Fracture length, x_f	Fracture width, w_f
1	237	0.007
2	594	0.007
3	260	0.008
4	250	0.009
5	257	0.008
6	528	0.005
7	371	0.008

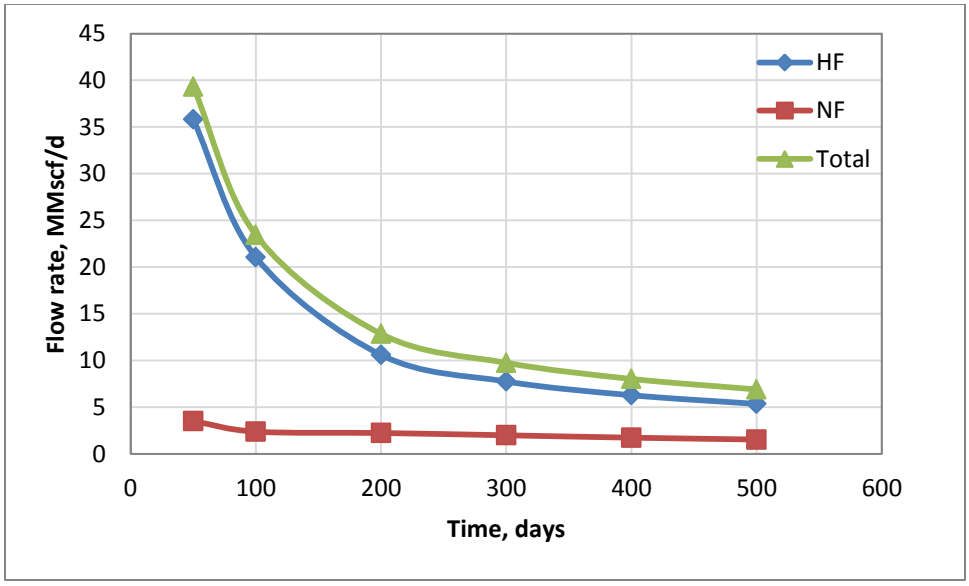

Fig. 38—Flow rate for complex fracture system.

4.1.5 Non-Darcy Flow

The Slab source solution model shows the effect of non-Darcy flow in the fracture. To understand the impact of the loss in fracture conductivity on well performance and cumulative gas production, we run case under transient condition. The results are compared with Miskimins and Barree's results (2005).

Three cases were run to show range producing conditions in low permeability reservoir. The specifics of these three cases are shown in **Table 12**. The five parameters are reservoir permeability, fracture proppant concentration, propped fracture height, BHFP, reservoir pressure, and propped fracture half-length. Each case was run with an effectively propped fracture half-length of 1000-ft, except for Case 2 which used x_f of 100-ft. No damage from filter-cake or gel residual in the pack was considered.

Table 12—Cases for non-Darcy flow study.

Case	Reservoir Perm (md)	Proppant Conc.	Frac Height (ft)	BHFP (psi)	Reservoir Pressure (pai)	x_f (ft)
1	0.01	1.0	100	1000	4000	1000
2	0.01	1.0	100	1000	4000	100
3	0.1	1.0	100	1000	4000	1000

The results of the three model cases are presented in **Fig. 39 thorough 41**. The models show that even for 0.01 md reservoirs the impact of non-Darcy flow can be significant if the created fracture length is long. In case 1, the slab source result shows a slightly higher production rate than Barree's results, but almost the same. The non-Darcy effects result decrease in cumulative production after 10 years of 11%.

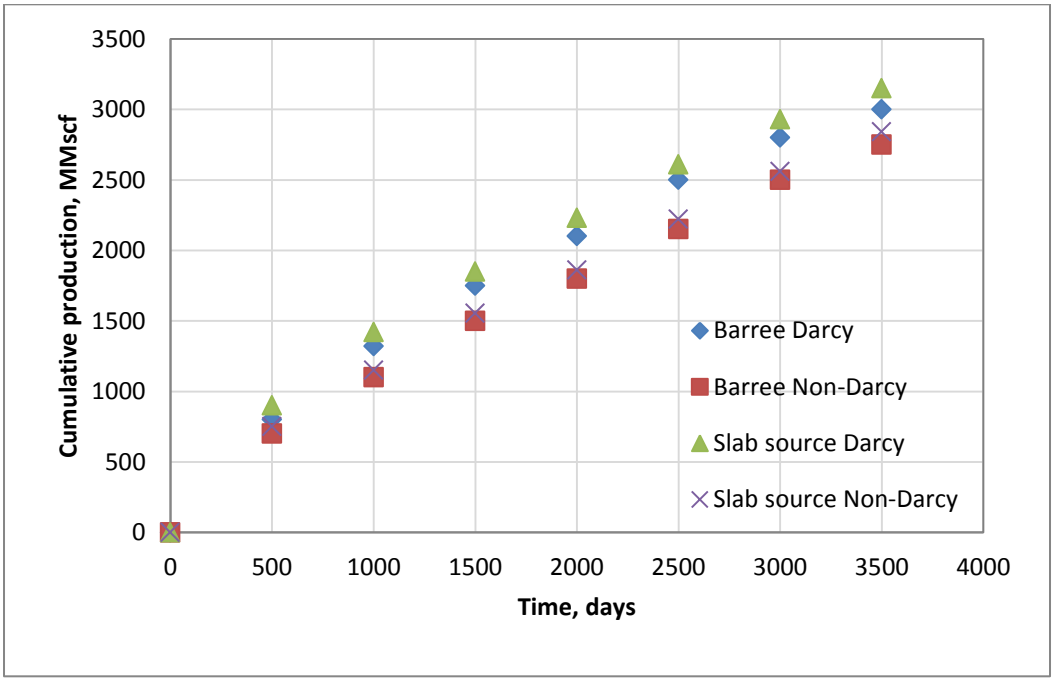

Fig. 39—Cumulative production for case 1.

Case 2 is similar to case 1 except that the fracture length is decreased from 1000-ft to 100-ft. when the fracture is short, **Fig. 40** shows that non-Darcy effects are not significant.

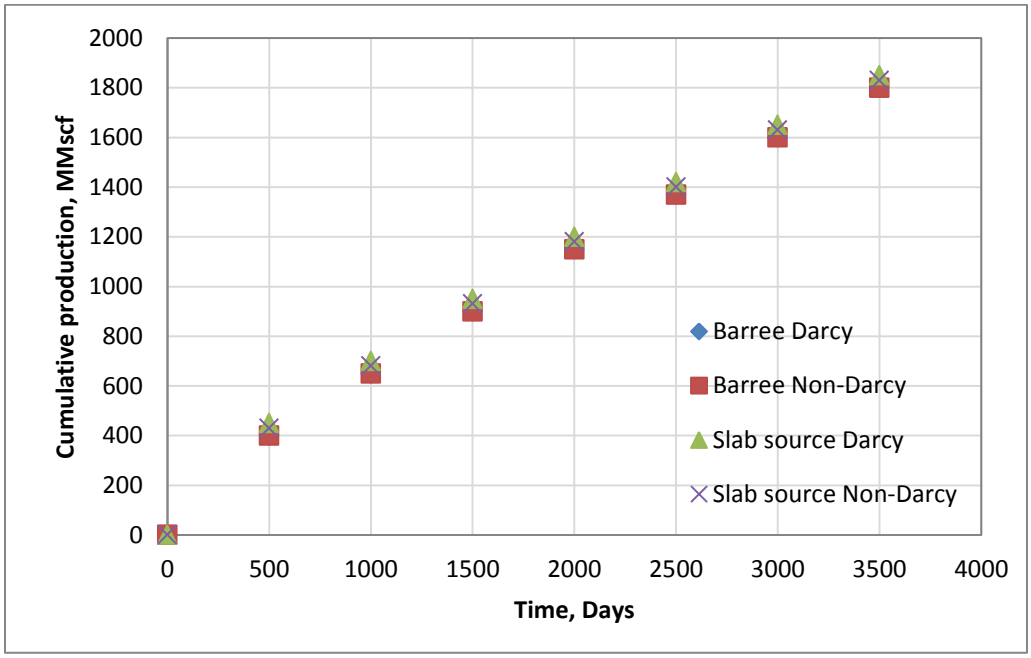

Fig. 40—Cumulative production for Case 2.

Fig. 41 shows the results for Case 3. This case the reservoir permeability is increase to 0.1-md. In this case the result shows that the non-Darcy flow effects are magnified. The difference in production after 10 years is 18%. The difference is caused by the high production which would introduce higher velocity, resulting in significant Non-Darcy flow effect.

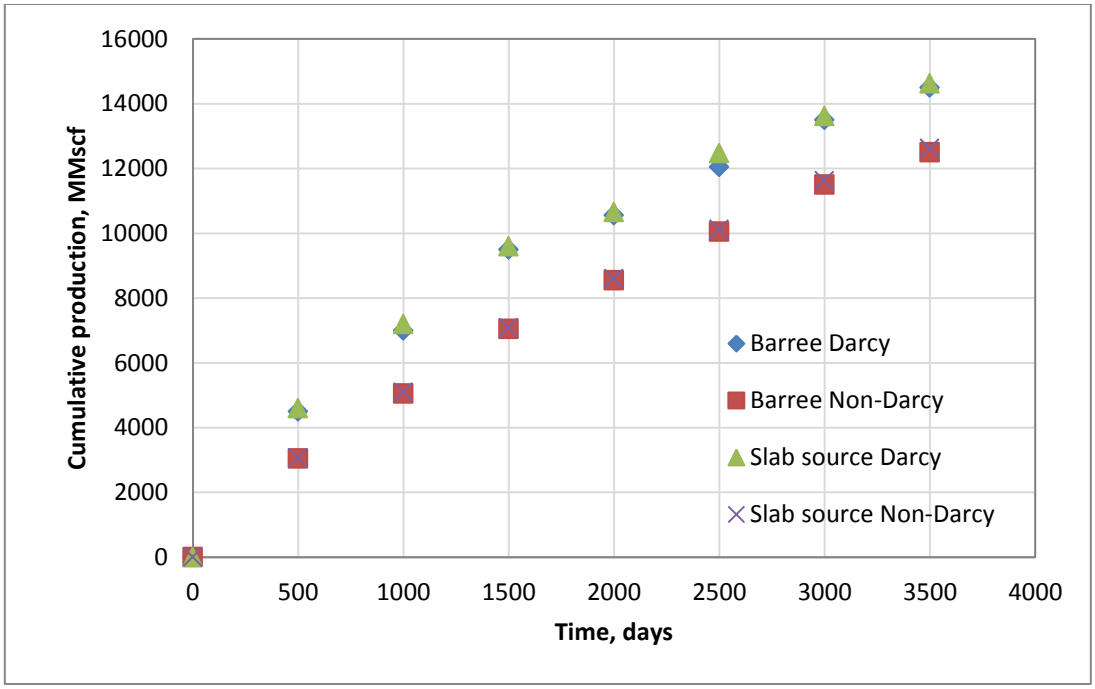

Fig. 41—Cumulative production for Case 3.

A summary of the 10-year cumulative production with and without non-Darcy flow effects for cases 1-3 is shown in **Table 13**. For the three cases shown, non-Darcy effects account for a range of 0.5% to 18% difference in cumulative production over ten years.

Table 13—Cumulative production results.

Case	Barree's model			Slab source Model		
No.	Darcy Flow (MMscf)	Non-Darcy (MMscf)	Percentage Change	Darcy Flow (MMscf)	Non-Darcy (MMscf)	Percentage Change
1	3160	2840	11.3	3250	2870	11.6
2	1835	1825	0.5	1850	1830	2.0
3	15000	12700	18.1	16100	12900	19.8

4.2 Field Cases

In this section, field examples are used to illustrate how to use the Slab model. Two field examples are used to show the procedure of the model application with one example for low permeability unconventional reservoir, and the other moderate permeability conventional reservoir.

4.2.1 Case1: Unconventional Reservoir (Mayer, shale)

To validate the multiple fracture calculation, we compared the model result with a published field production history data. The history match is based on a horizontal well in Marcellus shale as shown in **Fig. 42** (Meyer et al., 2010). The horizontal well was completed with a seven stage fracture treatment over a lateral length of 2100 ft. Seven stage fracture treatment was completed over the horizontal wellbore. The production log showed a total gas flow rate of 3.166 MMscf/d and a water rate of 2541 bpd. Stage two showed a minimal contribution of about 3% of the total production. Therefore, only six multiple transverse fractures were used to history match. The reservoir and fracture properties for Marcellus shale is given in **Table 14**. The Marcellus shale history matched parameters are given in **Table 15**.

Table 14—Marcellus Shale-reservoir and fracture properties.

Formation	Marcellus
Formation height, ft	162
Porosity, %	4.2
Pore Pressure, psi	4726
Specific Gravity	0.58
Temperature, °F	175
Drainage Area, acres	80
Reservoir Size (x_e,y_e), ft	933,3733
BHFP	1450-530
Wellbore Radius, ft	0.36
Well Length, ft	2100
Number of Stages	7

Table 15—History matched parameters.

Formation Permeability, k, md	0.000546
Fracture Permeability, k_f, md	526
Propped Length, ft	353
Fracture Width, ft	0.0065
Number Equivalent Fractures	6

The production data was matched with the single phase, multiple transverse fractures in horizontal wellbores, and the result is shown in **Fig. 43**. The history match analysis of measured production was based on the parameters which shown in **Table 15**. The calculated result is on the same order of the field observation. Because fractured well

performance depends on numerous parameters including reservoir properties and fracture geometries which both contain uncertainty and it is not surprised that a perfect match was not obtained. From the results (**Fig. 43**), the higher production rate at early time from the slab model could be caused by the assumptions of ideal condition of fractures and neglected Non-Darcy effect inside fracture. The proppant permeability used in the history match is the effective permeability. The effective permeability contains two parts, one is the proppant permeability and the other is the natural fracture permeability. In this case, the connection between natural fractures and hydraulic fractures are unknown factor, the source function cannot directly applied in the natural fracture system. The natural fracture permeability has been represented here as an effective proppant permeability in the hydraulic fractures.

An average permeability of 377 nanodarcy over a formation thickness of 162 ft that included the upper and lower Marcellus has been showed by a petrophysical analysis. The resulting reservoir capacity (kh) was calculated to be 0.061md-ft, an average reservoir permeability of 555 nanodarcy, and a reservoir capacity of 0.09 md-ft. the history match results for this case match very well with the information.

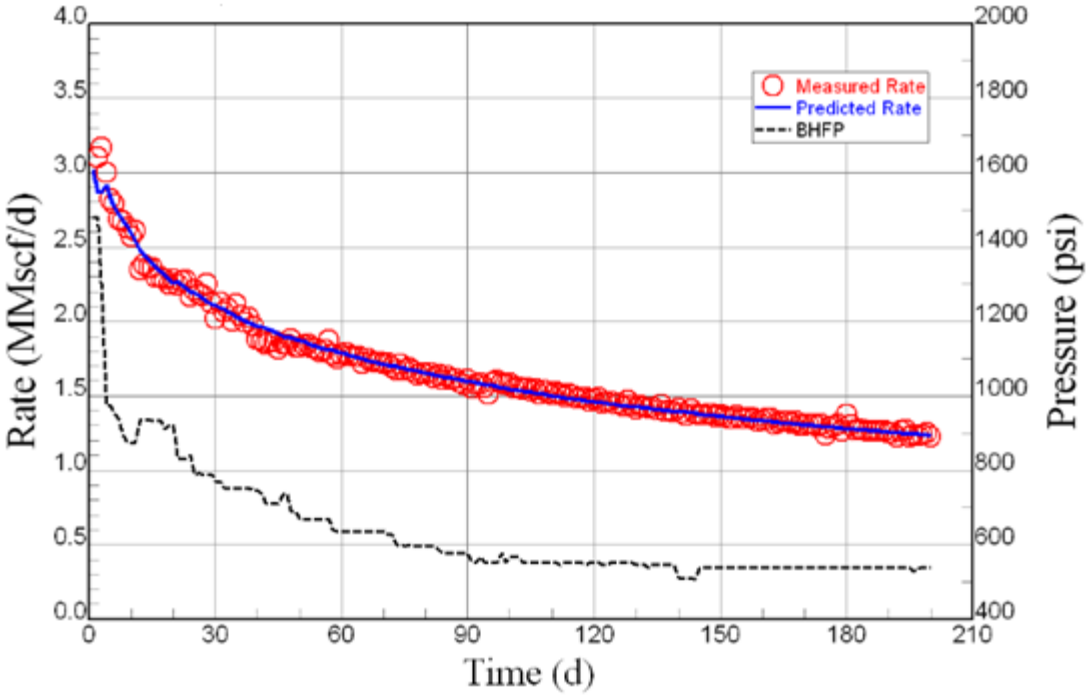

Fig. 42—Field Data (Meyer et al., 2010).

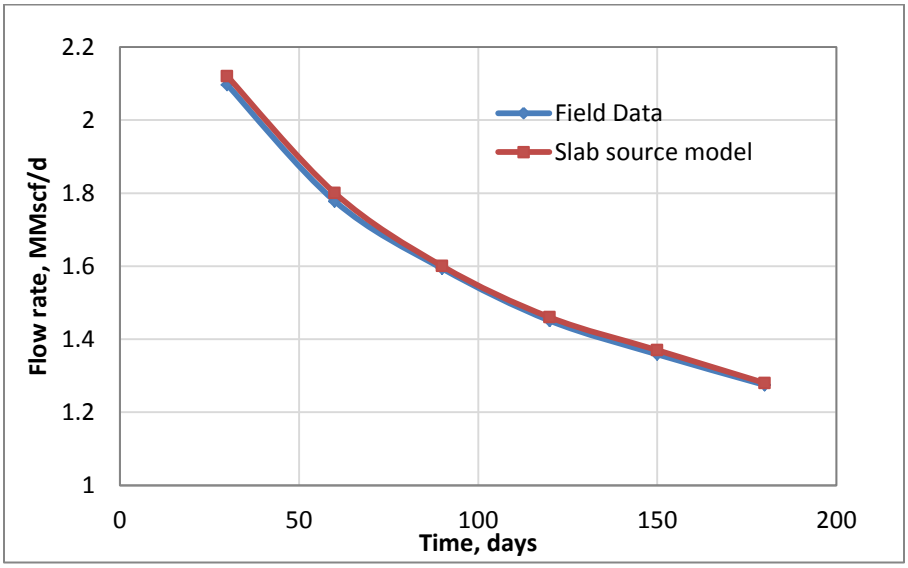

Fig. 43—History match of a gas well in Marcellus Shale.

4.2.3 Case2: Moderate Permeability

A gas reservoir is used in the example. The reservoir has multiple layers with significant contraction in permeability in each layer. The permeability profile is shown in **Table 16** and **Fig. 44**. Layer 3 has the lowest permeability, serving as a vertical isolation in the formation. In such a reservoir, horizontal well may lose its attraction compared with vertical well because of low vertical communication. The example compares the well structure plans including vertical well, vertical well with fracture, slanted well, horizontal well without fracturing, and horizontal well with multiple transverse fractures. The input data is shown in **Table 17**.

Table 16—Permeability summary for layers.

Layer No.	Layer Thickness (ft)	k_h (md)	k_v (md)	Average perm, k_h (md)
1	12	0.05-0.5	0.14	0.26
2	6	10.64	5.53	10.64
3	5	0.003	0.003	0.003
4	26	0.2-0.6	0.16	0.36
5	2	2.32	2.32	2.32
6	116	0.1-0.8	0.12	0.25
7	10	1.92	1.92	1.92
8	5	7.55	4.07	7.55
9	18	0.5-2.3	0.89	1.67

Table 17—Input data for case study.

Reservoir type	Tight gas	
Formation type	Sandstone	
Parameter	Value	Unit
Reservoir length (assumed), b	4000	ft
Reservoir width (assumed), a	2000	ft
Reservoir thickness, h	200	ft
Horizontal wellbore length, l	3000	ft
Porosity, ϕ	9.0%	
Reservoir initial pressure, p_i	2335	psi
Reservoir temperature, T	146	°F
Bottomhole pressure, p_{wf}	1886	psi
Gas specific gravity, γ_g	0.836	
Water specific gravity, γ_w	1.005	

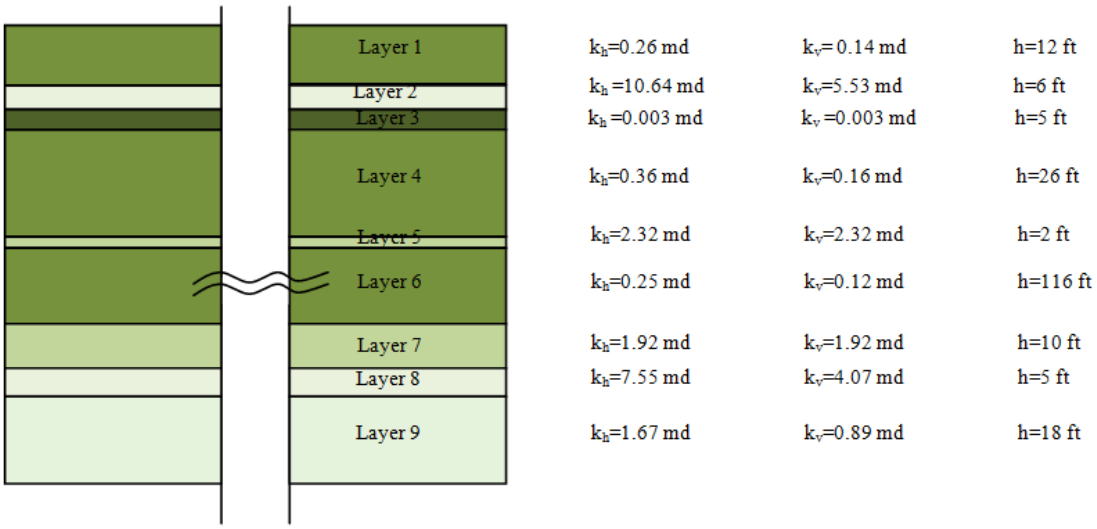

Fig. 44—Schematic of the formation.

Well Structure Design

Even vertical wells are considered as conventional and less aggressive, since this reservoir has multiple layers, vertical well should not be simply eliminated from consideration. The initial comparison considers a vertical well fully perforated in the pay zone as shown in **Fig. 45**, a hydraulic fractured vertical well with 500 ft fracture half-length (**Fig. 46**), and a 3000-ft long horizontal well (**Fig. 47**). One disadvantage of horizontal wells is that they could only produce from one pay zone. In such a heterogeneous reservoir, a slanted well with a deviated angle of 82° (**Fig. 48**) is considered here. To simplify the problem, the slanted well is approximated with three horizontal sections as shown in **Table 18**. The sum of the production from these sections provides us an estimated flow rate of a slanted well.

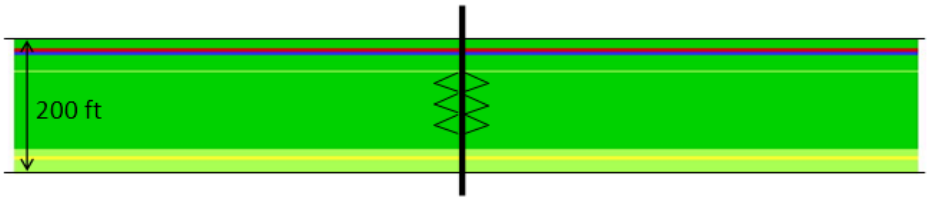

Fig. 45—Vertical well schematic.

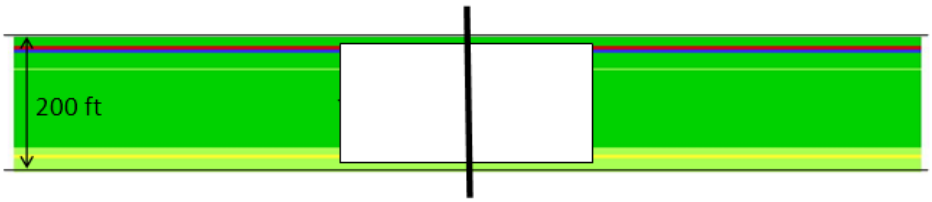

Fig. 46—Fractured vertical well schematic.

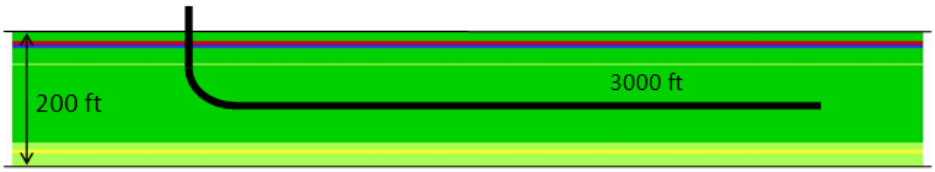

Fig. 47—Horizontal well schematic.

Table 18—Parameter list for slanted well.

Zone No.	Layer No.	k_h, md	k_v,md
1	1-4	0.72	0.34
2	5-6	0.26	0.2
3	7-9	1.67	0.92

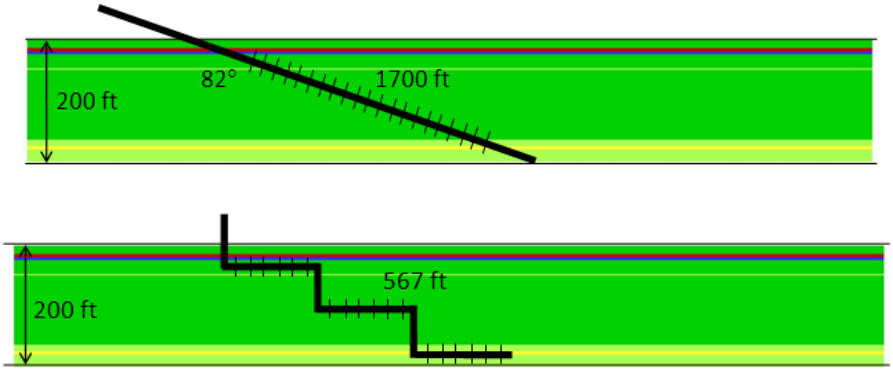

Fig. 48—Slanted well with 82° and modified well for simulation.

The last well plan is multiple transverse fractures along the horizontal well**.** Transverse fractures are equally placed along the horizontal well. Fracture numbers varied from 5 to 10. All the fractures have the same dimension of 500-ft in half length, 150 ft in height, and 0.033 ft in width.

Result Comparisons

The results of production rate for different well structures are shown in **Fig. 49.** From **Fig. 49**, it can be seen that the horizontal well with 10 fractures has the highest production rate since 10 fractures increase the contact with the reservoir most effectively and create the communication of the upper and the lower pay zones. However, the production rate declines significantly after 50 days. It also shows that the slanted well has the challenge production compared with the horizontal well and the fractured vertical well. Since the reservoir permeability is moderate for this gas formation, slanted well has the potential of improved production with relatively low cost compared with horizontal well and fracturing. **Fig. 50** shows the cumulative production. There are

significant increases in production from horizontal well/slanted well to horizontal well with 5 fractures. Economic evaluation is necessary to make final decision. This observation is directly related to the moderate permeability of the reservoir.

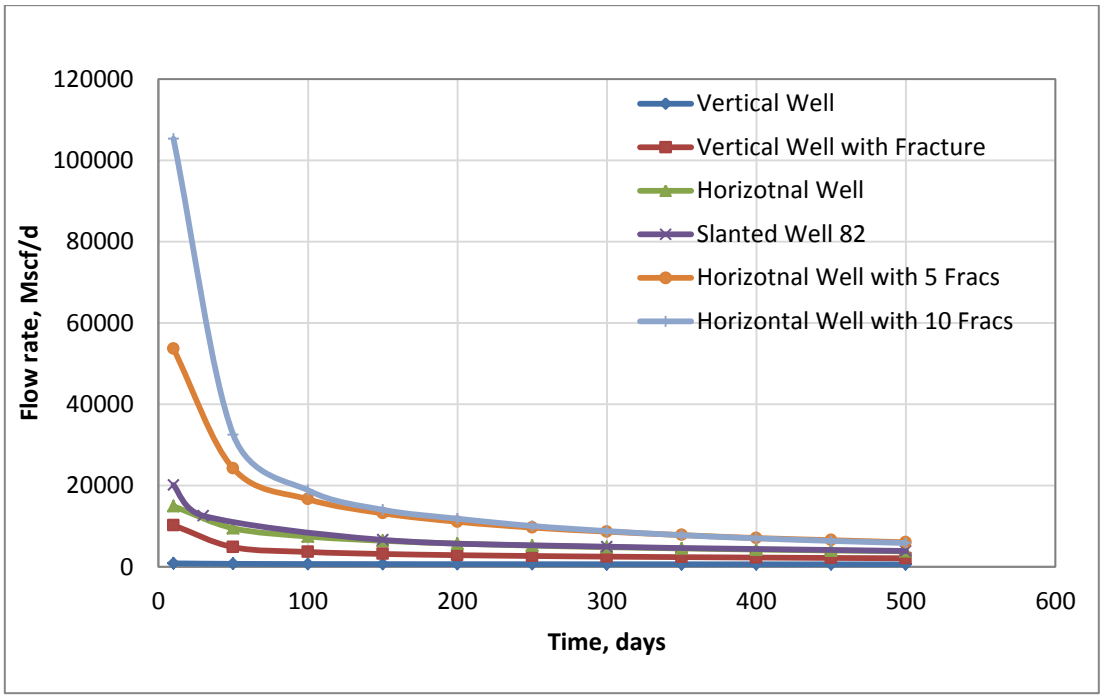

Fig. 49—Cases comparison for production rate.

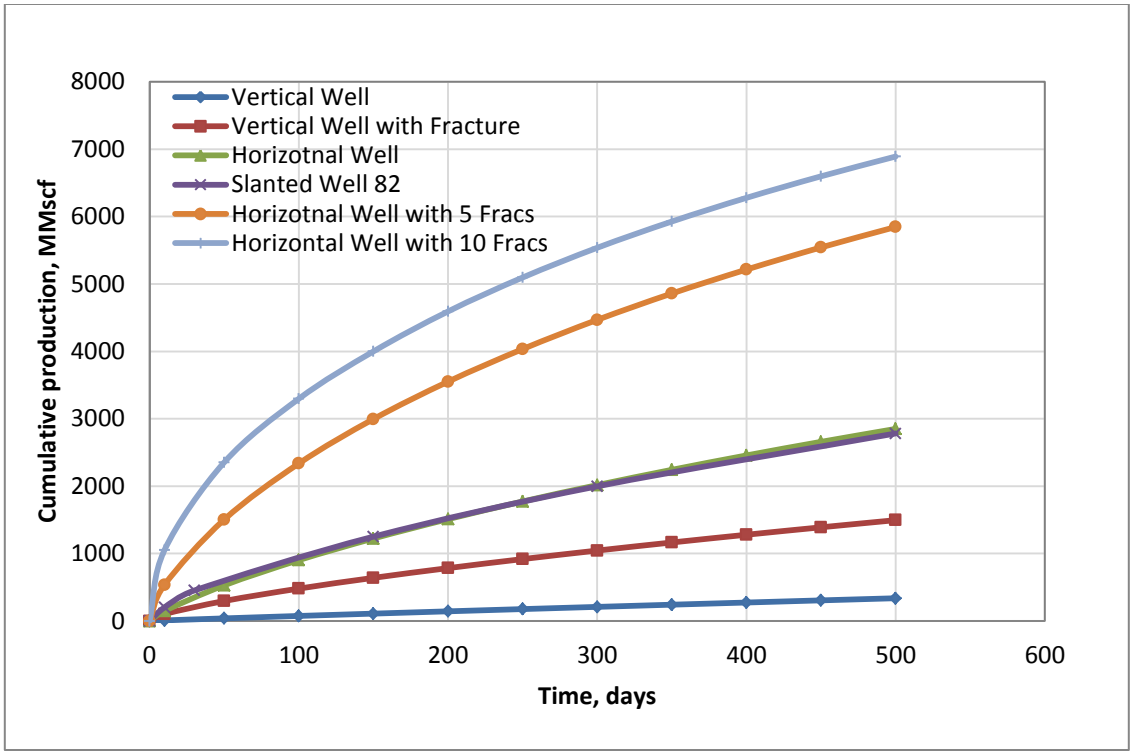

Fig. 50—Cases comparison for cumulative production.

CHAPTER V

CONCLUSIONS

Hydraulic fractures have been used widely today especially in the tight gas reservoir. Predicting well performance becomes much more difficult compared with conventional wells. In order to evaluate well performance, we developed a new model. This dissertation presents well performance models of horizontal wells with/without fractures, and complex fractures system. The model can be used to generate inflow performance relationships, study parameter sensitivity, and optimize well designs.

We developed the slab source method as a solution to calculation the well performance and pressure distribution in a closed, rectangular reservoir under different boundary conditions. The model can be used for both transient and pseudosteady-state flow. we have successfully developed and validated a series of solutions for pressure and production behavior of simple and complex well/fracture configurations such as horizontal well, multiple fractures, and natural fractures. We also demonstrated the applicability of the new solution method in predicting production behavior for a horizontal well with multiple transverse fractures and complex fractures system. The new method is applied as an optimization and screening tool to obtain the best completion schematic for development of well design.

The conclusions can be summarized as following:

1. Slab source model was developed successfully to calculate flow problems in complex reservoir system

2. Model can handle horizontal wells with multiple stage fractures in a natural fracture reservoir.
3. The optimal number of fracture stages is strongly depends on reservoir permeability. For moderate permeability formation, higher number of fractures stages does not necessarily yield justified benefit in production. For lower permeability formation, the higher the fracture number, the better the production. The optimal number of fractures should be determined by other constrains than production rate.
4. Non-Darcy flow effects have an influence on flow rates, these decrease can range from 2% to 20% under a given set of conditions.
5. Long-term production is significantly affected by Non-Darcy conductivity losses, even in relatively low permeability reservoirs where long fractures are needed.
6. For complex fracture system, the production from natural fractures depends on natural fracture location, dimension, and connection point with the hydraulic fractures.

Recommendations

Based on the results of this study, it is recommend that

1. Non-Darcy effects can be added for complex fractures system to count for the additional pressure and production decrease.
2. A comprehensive two-phase well flow model can be developed in the future.
3. The limitation of the model is that the natural fracture must be parallel to reservoir boundary.
4. Constant pressure boundary will be appreciated for application.

NOMENCLATURE

A_s	= cross-section area of source term, ft^2
a	= reservoir width, ft
B	= formation volume factor
b	= reservoir length, ft
c_t	= compressibility, psi^{-1}
h	= reservoir height, ft
k_x	= permeability in x-direction, md
k_y	= permeability in y-direction, md
k_z	= permeability in z-direction, md
l	= wellbore length, ft
L	=dimensionless reservoir position
p_D	=dimensionless pressure
p_{int}	= initial reservoir pressure, psi
p	= average reservoir pressure, psi
p_{wf}	= bottomhole pressure, psi
Δp	= pressure drawdown, psi
q	= flow rate, Mscf/day
T	= temperature, °R
t_D	=dimensionless time
x_D	= dimensionless reservoir length

x_f	= fracture width, fty_D
yf	=dimensionless reservoir width
z_D	=dimensionless reservoir height
γ_g	= specific gas gravity, dimensionless
ρ	= density, lb/ft^3
ϕ	= porosity, fraction
μ	= viscosity, cp
τ	= time
β	=$atm\text{-}sec^2/gm$
u_g	= cp or g/100-cm-sec

REFERENCES

Babu, D.K. and Odeh, A.S. 1988. Productivity of a Horizontal Well Appendices A and B. Paper SPE 18334 presented at the SPE Annual Technical Conference and Exhibition, Houston, Texas. 2-5 October.

Bagherian, B., Sarmadivaleh, M., Ghalambor, A., Nabipour, A., Rasouli, V. et al. 2010. Optimization of Multiple-Fractured Horizontal Tight Gas Well. Paper SPE 127899 presented at the SPE International Symposium and Exhibiton on Formation Damage Control, Lafayette, Louisiana, USA. 10-12 February.

Cinco-Ley, H. and Samaniego-V., F. 1981. Transient Pressure Analysis for Fractured Wells. *J. Pet Tech.* **33** (9): 1748-1766. SPE-7490-PA. DOI: 10.2118/

Cooke Jr., C.E. 1973. Conductivity of Fracture Proppants in Multiple Layers. *J. Pet Tech.* **25**(09): 1101-1107. SPE-4117-PA. DOI: 10.2118/4117-pa

Carslaw, H. S. and Jaeger, J. C. 1959. *Conduction of Heat in Solids*, Oxford, UK: Clarendon Press.

Cramer, D.D. 2004. Analyzing Well Performance in Hydraulically Fractured Gas Wells: Non-Ideal Cases. Paper SPE 90777 presented at the SPE Annual Technical Conference and Exhibition, Houston, Texas.26-29 September.

Darcy, H.P.G. 1856. *The Public Fountains of the City of Dijon (appendix)*. Bookseller of the Imperial Corps of Bridges, Highways and Mines, Quay of Augustins.

Ecrin-Kappa, User Manuel, Version 4.12, Sophia Antipolis, France.

Etherington, J.R. 2005. Getting Full Value from Reserves Audits. Paper SPE 95341 presented at the SPE Annual Technical Conference and Exhibition, Dallas, Texas. 9-12 October .

Forchheimer, P. 1901. *Wasserbewegung durch Boden*, Vol. 45. Zeits. V. Deutsch, Ing.

Geertsma, J. 1974. Estimating the Coefficient of Inertial Resistance in Fluid Flow through Porous Media. *SPE J.* **14** (5): 445-450. SPE-4706-PA DOI: 10.2118/4706-pa

Goode, P.A. and Kuchuk, F.J. 1991. Inflow Performance of Horizontal Wells. *SPE Res Eng* **6** (3): 319-323 SPE-21460-PA DOI: 10.2118/21460-pa

Gringarten, A.C. and Ramey Jr., H.J. 1973. The Use of Source and Green's Functions in Solving Unsteady-Flow Problems in Reservoirs. *SPE J.* **13** (5): 285-296. SPE-3818-PA. DOI: 10.2118/3818-pa.

Gringarten, A.C. and Ramey Jr., H.J., and Raghavan, R. 1974. Unsteady-State Pressure Distribution Created by a Well With a Single Infinite-Conductivity Vertical Fracture. *SPE J.* **14** (4): 347-360. SPE-4051-PA. DOI: 10.2118/4051-pa.

Meyer, B.R., Bazan, L.W., Jacot, R.H., and Lattibeaudiere, M.G. 2010. Optimization of Multiple Transverse Hydraulic Fractures in Horizontal Wellbores. Paper SPE 131732 presented at the SPE Unconventional Gas Conference, Pittsburgh, Pennsylvania, USA. 23-25 February.

Miskimins, J.L., Lopez, H.D.J., and Barree, R.D. 2005. Non-Darcy Flow in Hydraulic Fractures: Does It Really Matter? Paper SPE 96389 presented at the SPE Annual Technical Conference and Exhibition, Dallas, Texas. 9-12 October.

Ouyang, L.-B., Thomas, L.K., Evans, C.E., and Aziz, K. 1997. Simple but Accurate Equations for Wellbore Pressure Drawdown Calculation. Paper SPE 38314 presented at the SPE Western Regional Meeting, Long Beach, California. 25-27 June.

Ozkan, E., Sarica, C., Haciislamoglu, M., and Raghavan, R. 1995. Effect of Conductivity on Horizontal Well Pressure Behavior. *SPE Advanced Technology Series* **3** (1): 85-94. SPE-24683-PA. DOI: 10.2118/24683-pa

Penny, G.S. and Jin, L. 1995. The Development of Laboratory Correlations Showing the Impact of Multiphase Flow, Fluid, and Proppant Selection Upon Gas Well Productivity. Paper SPE 30494 presented at the SPE Annual Technical Conference and Exhibition, Dallas, Texas. 22-25 October.

Roussel, N. P., and Sharma, M. M., 2010. Optimizing Fracture Spacing and Sequencing in Horizontal Well Fracturing. Paper SPE 127986 presented at SPE International Symposium and Exhibition on Formation Damage Control , Lafayette, Louisiana, USA. 10-12 February.

Smith, M.B., Bale, A., Britt, L.K., Cunningham, L.E., Jones, J.R. et al. 2004. An Investigation of Non-Darcy Flow Effects on Hydraulic Fractured Oil and Gas Well Performance. Paper SPE 90864 presented at the SPE Annual Technical Conference and Exhibition, Houston, Texas. 26-29 September.

Suri. A., and Sharma, M.M., 2009. Fracture Grouwth in Horiozntal injectors. Paper SPE 119379 presented at SPE Hydraulic Fracturing Technology Conference, Woodlands, Texas, USA. 19-21 January.

Valko, P.P. and Amini, S. 2007. The Method of Distributed Volumetric Sources for Calculating the Transient and Pseudosteady-State Productivity of Complex Well-Fracture Configurations. Paper SPE 106279 presented at the SPE Hydraulic Fracturing Technology Conference, College Station, Texas USA. 29-31 January.

Zhu, D., Magalhaes, F.V., and Valko, P. 2007. Predicting the Productivity of Multiple-Fractured Horizontal Gas Wells. Paper SPE 106280 presented at the SPE Hydraulic Fracturing Technology Conference, College Station, Texas USA. 29-31 January.

APPENDIX A

The use of Green's functions in the theory of potential is well known. The function is most conveniently defined for the closed surface S as the potential which vanishes over the surface, and is infinite as 1/r, when r is zero, at the point p(x',y',z') inside the surface. If this solution of the equation $\nabla^2 u = 0$ is denoted by G(p). The solution with no infinity inside S and an arbitrary value V over the surface is given by

$$\mu = \frac{1}{4\pi}\iint \frac{\partial}{\partial n} G(p) V dS \qquad \text{A1}$$

$\frac{\partial}{\partial n}$ denoting differentiation along the outward drawn normal.

We proceed to show how a similar function may be employed with advantage in the mathematical theory of the conduction of heat. In this case we shall take the Green's function as the temperature at (x,y,z) at the time t, due to an instantaneous point source of strength unity generated at the point p(x',y',z') at time τ, the solid being initially at zero temperature, and the surface being kept at zero temperature. This solution is written

$$\mu = F(x, y, z, x', y' z', t - \tau) \qquad (\tau > t) \qquad \text{A2}$$

and u satisfies the equation

$$\frac{\partial \mu}{\partial t} = k\nabla^2 u \qquad (\tau > t) \qquad \text{A3}$$

However, since t only enters in the form (t-τ), we have also

$$\frac{\partial \mu}{\partial t} + k\nabla^2 u = 0 \qquad (\tau < t) \qquad \text{A4}$$

Further, $\lim_{t \to \tau}(u) = 0$ at all points inside S, expect at point (x',y',z'), where the solution takes the from

$$\frac{1}{8[\pi k(t-\tau)]^{3/2}} \exp\left(\frac{-(x-x')^2 + (y-y')^2 + (z-z')^2}{4k(t-\tau)} \right) \qquad \text{A5}$$

Finally, at the surface S, u=0 (τ<t).

Let v be the temperature at the time t in this solid due to the surface temperature ϕ(x,y,z,t) and the initial temperature f(x,y,z)

Then v satisfies the equations

$$\frac{\partial v}{\partial t} = k\nabla^2 v \qquad (t>0) \qquad \text{A6}$$

v=f(x,y,z) inially, inside S

v=ϕ(x,y,z) at S, when t>0

Also, since the time τ of our former equations lies within the interval for t, we have

$$\frac{\partial v}{\partial t} = k\nabla^2 v \qquad (\tau<t) \qquad \text{A7}$$

v=ϕ(x,y,z) at the surface.

Therefore,

$$\frac{\partial(uv)}{\partial t} = u\frac{\partial v}{\partial \tau} + v\frac{\partial u}{\partial \tau} = k\left(u\nabla^2 v - v\nabla^2 u\right) \qquad \text{A8}$$

and

$$\int_0^{t-\varepsilon} \left(\iiint \frac{\partial(uv)}{\partial \tau} dxdydz \right) d\tau = k \int_0^{t-\varepsilon} \iiint \left(u\nabla^2 v - v\nabla^2 u\right) dxdydzd\tau \qquad \text{A9}$$

The triple integrate being taken into the solid, and ε being any positive number less than t.

Interchanging the order of integration on the left-side of this equation and applying Green's theorem to the right-hand side. We have

$$\iiint (uv)_{\tau=t-\varepsilon}\, dxdydz - k\iiint (uv)_{\tau=0}\, dxdydz$$

$$= k\int_0^{t-\varepsilon}\left[\iint\left(u\frac{\partial v}{\partial n} - v\frac{\partial u}{\partial n}\right)dS\right]d\tau$$

$$= k\int_0^{t-\varepsilon}\left[\iint v\left(\frac{\partial u}{\partial n}\right)_i dS\right]d\tau \qquad \text{A10}$$

where $\frac{\partial}{\partial n_i}$ denotes differentiation along the inward-drawn normal, and we have used the condition that u vanishes at the surface.

Now take the limit as ε tends to zero. The left-side gives

$$[V_P]_\tau \iiint u_{\tau=t}\, dxdydz - \iiint u_{\tau=0} v_{\tau=0}\, dxdydz \qquad \text{A11}$$

The first integral being taken though an element of volume including the point p(x',y',z'), where the function u becomes infinite at t=τ. The second integral being taken through the solid, and the $[V_P]_\tau$ stands for the value of v at the point p(x',y',z') at the time t. but since u is the temperature at the time t due to a unit source at (x',y',z') at time τ, $\iiint u_{\tau=t}\, dxdydz = 1$ and we have

$$[V_P]_\tau = \iiint u_{\tau=0} v_{\tau=0}\, dxdydz + kt\int_0^{t-\varepsilon}\left[\iint v\left(\frac{\partial u}{\partial n}\right)_i dS\right]d\tau$$

$$= \iiint u_{\tau=0} f(x,y,z)dxdydz + kt\int_0^{t-\varepsilon}\left[\iint \phi(x,y,z,\tau)\left(\frac{\partial u}{\partial n}\right)_i dS\right]d\tau \qquad \text{A12}$$

as the temperature at (x',y',z') at the time t due to the initial distribution f(x,y,z) and the surface temperature ϕ(x,y,z,t).

In the case of radiation at the surface, the Green's function u is taken as the temperature at (x,y,z) at time t due to an instantaneous point source of strength unity generated at (x',y',z') at time τ, radiation taking place at the surface into a medium at zero temperature.

Linear flow in the semi-infinite solid x>0

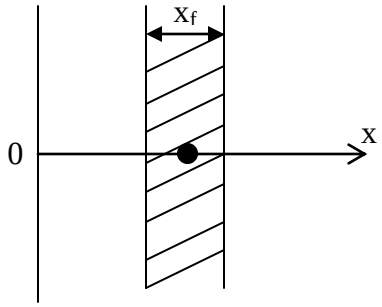

Fig. 51—Semi-infinite solid reservoir and slab source.

The solution is

$$\frac{1}{\sqrt{4\pi k(t-\tau)}}\int_{x_w-\frac{x_f}{2}}^{x_w+\frac{x_f}{2}} \exp\left[-\frac{(x-x')^2}{4k(t-\tau)}\right]dx' \qquad \text{A13}$$

For linear flow in reservoir, 0<x<a, the slab source is at $x=x_w$ as shown in . Initial temperature f(x), bounding planes kept at zero.

Starting with the source $f(x_w)dx_w$ at x_w, we have to take the images of this source in the planes x=0 and x=a, a source and a sink alternating so that the boundaries may be kept at zero. In this way we have sources at the points x_w+2na and sinks at the points $–x_w+2na$, where n is zero or any positive or negative integer.

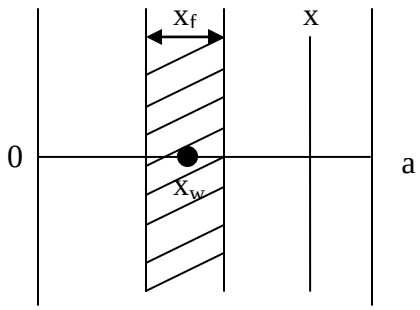

Fig. 52—Finite solid bounded by the planes x=0 and x=a, slab source.

Thus, we have finally

$$v=\frac{1}{\sqrt{4\pi k(t-\tau)}}\left\{\sum_{n=-\infty}^{\infty}\int_{x_w-\frac{x_f}{2}}^{x_w+\frac{x_f}{2}}\exp\left[-\frac{((x-2na)-x')^2}{4k(t-\tau)}\right]dx'\right.$$

$$\left.+\sum_{n=-\infty}^{\infty}\int_{x_w-\frac{x_f}{2}}^{x_w+\frac{x_f}{2}}\exp\left[-\frac{((x-2na)+x')^2}{4k(t-\tau)}\right]dx'\right\} \qquad \text{A14}$$

Because of the Poisson's summation formula,

$$\sum_{n=-\infty}^{\infty}\exp\left[-\frac{\left((x-2na)-x'\right)^2}{4k(t-\tau)}\right]=\frac{\sqrt{\pi k(t-\tau)}}{a}\left[1+2\sum_{n=1}^{\infty}\cos\frac{n\pi(x-x')}{a}e^{\frac{-kn^2\pi^2t}{a^2}}\right]$$

$$\sum_{n=-\infty}^{\infty}\exp\left[-\frac{\left((x+2na)-x'\right)^2}{4k(t-\tau)}\right]=\frac{\sqrt{\pi k(t-\tau)}}{a}\left[1+2\sum_{n=1}^{\infty}\cos\frac{n\pi(x+x')}{a}e^{\frac{-kn^2\pi^2t}{a^2}}\right] \quad \text{A15}$$

Therefore, A14 could be written as

$$v=\frac{x_f}{a}\left\{1+\frac{4a}{\pi x_f}\sum_{n=1}^{\infty}\frac{1}{n}\exp\left[-\frac{\pi^2n^2k(t-\tau)}{a^2}\right]\sin\frac{n\pi x_f}{2a}\cos\frac{n\pi x_w}{a}\cos\frac{n\pi x}{a}\right. \quad \text{A16}$$

VITA

Jiajing Lin received her Bachelor of Science degree in electronic engineering from Beijing Institute of Technology in 2004. She attended the petroleum engineering program at the University of Louisiana at Lafayette in September 2004 and received her Master of Science degree in August 2006. After that, she entered in the engineering school at Texas A&M University and completed her Ph.D. in petroleum engineering in 2011.

She may be reached at:

Department of Petroleum Engineering

Room 712, RICH Building

College Station, TX 77843-3116

Her Email is tumi.lin@gmail.com